ELECTROPHORETIC DEPOSITION AND CHARATERIZATION OF CHITOSAN/ SILICA/ BIOACTIVE GLASS COMPOSITE COATINGS ON MAGNESIUM WE43 ALLOY

AUTHOR: Joan Franco Gagliardo

SUPERVISORS: Dr. Josefina Ballarre
Dr. Aldo Bocaccini

Materials Engineering

Universidad Nacional de Mar del Plata- Facultad de Ingeniería
Friedrich-Alexander Universität Erlangen-Nürnberg

May 2017

UNIVERSIDAD NACIONAL DE MAR DEL PLATA

FACULTAD DE INGENIERIA

FRIEDRICH-ALEXANDER UNIVERSITÄT ERLANGEN-NÜRNBERG
TECHNISCHE FAKULTÄT

INDEX

RESUMEN EN ESPAÑOL

El magnesio y sus aleaciones se presentan como promisorios materiales en el campo de la medicina como implantes temporarios debido a sus propiedades mecánicas, degradabilidad y biocompatibilidad. El objetivo principal de los implantes temporarios es proveer de propiedades mecánicas similares a las del hueso en su estado original y lograr que el hueso se regenere antes de la degradación completa del implante. La velocidad de degradación del material, con la consecutiva pérdida en las propiedades mecánicas, tiene que ser acorde con la velocidad de crecimiento y regeneración del hueso, hasta que el mismo sea capaz de soportar las solicitaciones mecánicas que soporta el tejido óseo como sostén por sí mismo. Las desventajas del Mg y sus aleaciones son: -la baja resistencia al desgaste. –Degradación rápida y no homogénea. – Formación de hidrógeno durante la corrosión, cambiando el pH en la vecindad de la superficie [1][2][3].Lo anterior puede llevar a que, para el momento en el cual el implante se degradó completamente, el hueso todavía no posea las propiedades mecánicas requeridas.

Existen dos formas de mejorar el comportamiento a la corrosión del Mg y sus aleaciones: -Ajustando la composición y microestructura y/o generando un recubrimiento del material con capas protectoras de cerámico, polímero o materiales compuestos. Debido a la baja solubilidad de muchos elementos en el Mg, los recubrimientos resultan de gran atracción para la mejora del control de la corrosión [4].

La deposición electroforética (EPD) es un proceso de producción de una capa a partir de una solución coloidal, en el cual las partículas suspendidas en el medio líquido migran bajo la influencia de un campo eléctrico (electroforesis) y consecuentemente se depositan en el electrodo hacia el cual están atraídas. Esta técnica se caracteriza por tener múltiples ventajas, entre ellas: bajo tiempo de deposición, aplicabilidad a cualquier sólido en forma de polvo fino o suspensión coloidal, simplicidad del equipo y poca restricción en la forma de los substratos. Aquellas características permiten que el EPD sea una técnica simple, versátil y con una relación costo-beneficio adecuada para la generación de recubrimientos en aplicación biomédica [5].

El quitosano es un polisacárido natural catiónico que puede ser producido por la deacetilenación de la quitina. Propiedades como la actividad antimicrobial, estabilidad química, biocompatibilidad y propiedades mecánicas avanzadas, le otorgan significativa importancia en el área de biotecnología. Los recubrimientos con vidrios bioactivos son comúnmente utilizados en ingeniería de tejidos debido a que las partículas de bio-vidrio promueven la interacción hueso-implante y crecimiento de hueso. Aquellas propiedades son atribuidas a la liberación de iones específicos y a la formación de una capa de hidroxiapatita en su superficie, la cual sirve de substrato

bioactivo para que las células madres pueden anexarse y diferenciarse [6]. La estructura hibrida (colágeno - apatita) natural del hueso inspiraron a la creación de recubrimientos compuestos por polímeros biodegradables/vidrios bioactivos para implantes ortopédicos [7]. Una forma de mejorar la performance de la capa de quitosano/Bioglass®, en términos mecánicos y/o bioactivos, es con la adición de refuerzos nanoparticulados. Un posible refuerzo es mediante partículas de PHBV (poli (3-hidroxibutirato-co-3-hidroxivalerato)) o de sílice amorfo. Las nano partículas de sílice también se piensa que pueden tener un rol potencial en la aceleración de los procesos de mineralización del hueso, resultando atractivo su uso para aplicaciones biomédicas[8].

La superficie de los recubrimientos compuestos por quitosano/ partículas de sílice/ vidrio bioactivo depositados sobre la aleación de magnesio WE43 fueron caracterizados a través de microscopía óptica, SEM, ángulo de contacto, test de rugosidad y tape test (ensayo para evaluar la adhesión cualitativa). Para evaluar el comportamiento bioactivo del recubrimiento, se llevó a cabo la inmersión de las muestras durante diferentes tiempos en un líquido que posee concentraciones de iones similares a las del fluido corporal (*Simulated Body Fluid* ó SBF) a 37°C. Posteriormente, las muestras fueron caracterizadas por medio de microscopía óptica, SEM, FTIR, espectroscopia Raman y DRX con el objetivo de determinar la formación de hidroxiapatita carbonatada. La caracterización frente al comportamiento a la corrosión fue llevada a cabo a través de ensayos electroquímicos, tales como espectroscopia de impedancia electroquímica y polarización anódica potenciodinámica en 0.1 M NaCl a temperatura ambiente.

Como conclusiones particulares del proyecto final se detallan:

- Las partículas de sílice fueron exitosamente sintetizadas. El control de los reactivos involucrados en el método sol-gel posibilitó la síntesis de partículas de sílice esféricas, monodispersas y del tamaño deseado.
- Los recubrimientos compuestos por quitosano/sílice/vidrio bioactivo fueron depositados en la aleación de magnesio WE43 a través de deposición electroforética. La variación de los parámetros de deposición dentro del rango 15-85V y 20-90 segundos permitieron analizar y seleccionar, a través de microscopía óptica y SEM, el mejor recubrimiento multi - capa.
- Mediante diferentes métodos de análisis (difractivos, espectroscópicos y electrónicos), se logró la identificación de hidroxiapatita carbonatada, principal componente inorgánico del hueso y primer indicio de bioactividad, después de 7 días de inmersión de las muestras recubiertas en SBF a 37°C.
- Los ensayos electroquímicos hicieron posible determinar que el recubrimiento no provee mejoras al substrato en la protección contra la corrosión, por lo menos hasta 30 minutos de inmersión de las muestras en 0.1M NaCl a temperatura ambiente.

ACKNOWLEDGMENTS

First of all, I would like to thank Aldo Bocaccini and Silvia Simison for giving me the incredible opportunity to participate in the I.DEAR program between Germany and Argentina. Thanks to Aldo Bocaccini for letting me investigate and work in this project at the Institute of Biomaterials of Erlangen. Certainly, the exchange program was the best experience of my life, which I will never forget and which allowed me to grow and develop myself not only in a professional way but also in a personal aspect.

I would like to thank also to Josefina Ballarre and Silvia Ceré for all the knowledge they shared with me and for supervising, guiding, helping me during this part of the final project at the División Electroquímica Aplicada of INTEMA –CONICET-UNMdP, for providing me advices every time I needed it, for being so kind, friendly and for giving me all the resources as possible to make me feel comfortable. I am extremely grateful and happy to have gone through this stage with them. My gratitude to all the people conforming the División Electroquímica Aplicada for their kindness.

Thanks to Svenja Heise for supervising me during my stay at the Institute of Biomaterials of Erlangen. Special thanks to Vanesa Fuchs, Sergio Pellice and Mariela Desimone for technical and theoretical support and for being willing to help every time they could.

Thanks to all my friends for being there for me, especially to those I have met during these 6 years of university. For all the meetings, laughs, happy hours to release university stress, for sharing deadlines, trips and for sharing this adventure with me.

Finally but not last, I would like to thank to my family, the strong pillars of my life: mamá, papá, Giuly y Luisi. Thanks for being understandable, for making me the way so easy, for encouraging me and for motivating me to pursuit whatever I want to achieve in life. For making me the person I am today.

1 ABSTRACT

Magnesium (Mg) and its alloys have been extensively explored as potential biodegradable implant materials for orthopedic and dental applications. However, the rapid degradation corrosion of Mg based alloys in physiological conditions has delayed their introduction for therapeutic applications. Electrophoretic deposition (EPD) of chitosan/silica/ bioactive glass (45S5 composition) composite coating on magnesium alloy (WE43) substrates was investigated. The present project has the aim to reduce and control the substrate corrosion rate and augment the initial bioactivity. The surface morphology, hydrophilic character, adhesion and surface topography of the coated sample were investigated by means of optical microscopy, SEM images, contact angle, roughness and tape test. The *in vitro* test consisted on immersion of the coated samples in Simulated Body Fluid (SBF) at 37°C during 2h, 1, 2, 3 and 7 days with following characterization through optical microscopy, SEM, Fourier Transform Infrared Spectroscopy (FTIR), Raman spectroscopy and X-Ray Diffraction (XRD) in order to identify hydroxycarbonate apatite (HCA) formation on the surface. HCA indicates the degree of bioactivity of the sample, because it leads to strong bond between the biomaterial and the living tissue. Characterization of the corrosion behavior was achieved by electrochemical impedance spectroscopy (EIS) and by potentiodynamic polarization in 0.1 M NaCl at ambient temperature.

Surface analysis of the coated sample showed to be beneficial for bone regeneration. HCA formation was confirmed after 7 days of immersion in SBF, providing a bioactive behavior to the Mg WE43 alloy. Regarding the degradation behavior, results showed that the coating did not provided improvements on protection against corrosion at least during the 30 minutes that the samples were immersed in 0.1M NaCl at ambient temperature.

2 INTRODUCTION

2.1 IMPLANT MATERIALS

Different types of materials can be used as implant materials: metals, polymers, glasses, ceramics and composites. The selection of a material for a specific implant depends, among others, on the anatomical location. Anyhow, all of them have to fulfill the requirement of not generating an adverse reaction once within the body.

The most accepted definition of biomaterials is the one employed from the health care perspective as: “materials those possess some novel properties that make them appropriate to come in immediate contact with the living tissue without eliciting any adverse immune rejection reactions” [9].

An adequate selection of the implant biomaterial is a key factor for long term success of implants. The biologic environment does not accept completely any material so to optimize biologic performance implants should be selected to reduce the negative response while maintaining appropriate function.

All of the biomaterials employed for hard and soft tissue applications have to fulfill the following requirements [10]:

- Biocompability, i.e.: The material does not interact adversely with the physiological environment or vice versa.

- Surface texture matching cellular adhesion without relative interfacial motion.

- Biofunctionality, e.g. mechanical requirements, which may differ for bone, soft tissue and vascular prostheses.

- Exhibit corrosion resistance, in order to maintain mechanical properties and low material dissipation out to tissues and excreting organs.

- Bioadhesion; a chemical, electrostatic, mechanical or combined bond between the prosthesis and surrounding tissue must have evolved after an appropriate healing period in order to avoid a fibrous encapsulation of the implant (related to surface texture and tissue-implant chemistry).

- Prevention of bacterial adhesion and/or facilitation of bacteria killing.

- Low price and processability are desirable.

When a biomaterial is placed within the human body, tissue reacts towards the implant in three different ways depending on the material type. If there is any tissue reaction it would be in response to the implant surface. These materials are classified in [11]:

- Inert: which the tissue forms a non-adherent and fibrous capsule around the implant. The body recognizes the implant as foreign and tries to isolate it by forming the capsule, as an immunological response.

- Degradable: which the tissue replaces them after a period of time and their function within the body is temporary.

- Bioactive: which have the property of establishing chemical bond with bone tissue (osseointegration) through an ion exchange reaction between the implant and the surrounding body fluid. The collagen and mineral phase of the adjacent bone is deposited directly on the implant surface.

Once within the body, the first contact is between the implant surface and the water molecules of the biological fluid, which occurs in nanoseconds. After that, ions are absorbed, and after a few seconds proteins cover the surface. Finally, between some minutes and a few hours, different kind of cells will approach the material, already covered by a protein layer. At the same time, bacteria can compete with the cells for further colonization [12].

A pre-requisite criterion for a successfully implant integration depends on a series of procedure-related and patient-dependent measures. From the clinical stand-point, successful osseointegration is a measure of implant stability, which occurs after implant integration. Primary stability is associated with the mechanical engagement of an implant with the surrounding bone, whereas bone regeneration and remodeling determine the secondary (biological) stability to the implant. A secure primary stability is positively associated with a secondary stability. Primary stability is accomplished when the implant is in located in a fixed position, allowing the implant to mechanically adapt to host bone. In one hand, the factors that affect this adaption are: bone quantity and quality, surgical technique and implant design. Implant design refers to the three dimensional structure of an implant with all the components and features that characterize it. On the other hand, the factors that influence the secondary stability are bone remodeling, implant surface conditions and the primary stability [13].

2.1.1 Metals for biomedical application

Metallic materials play and essential role as biomaterials to assist with the repair or replacement of bone tissue that has become diseased or damaged. Compared to ceramic or polymeric materials, metals are more suitable for load-bearing applications due to their combination of high mechanical strength and fracture toughness. These are the reasons why nowadays metals are used on applications regarding permanent or temporary implants. Traditionally, permanent metallic implants have consisted of titanium and its alloys, stainless steel and cobalt, chromium and nickel base alloys [14]. Certain limitations of these materials are the possible release of toxic metallic

ions and/or particles through corrosion or wear processes, reducing their biocompatibility and causing inflammatory reactions and tissue loss. Besides, generally and in most cases, there is a mismatch between the bone tissue and the biomaterial´s elastic moduli , resulting in stress shielding that can lead to reduced stimulation of new bone growth and remodeling (decreasing implant stability) [15].

2.1.1.1 Magnesium WE43 alloy

Magnesium has been suggested as a revolutionary temporary implant material to overcome the limitations of the permanent metallic implants previously mentioned [14]. Mechanical properties of Mg in comparison with bone are listed in Table 1. Mg is light in weight and low in density, and exhibits high strength to weight ratio. The elastic modulus of Mg is really close to the cortical bone´s one, and this property represents an advantage among the other metallic implants due to a decrease in stress shielding. In addition, Mg also has the advantage of degradation and thus, if corrosion rate is controlled, the material would slowly degrade at the same time that bone healing process is taking place, until the bone itself has the capability of supporting the stresses associated to that anatomical place. Moreover the need of a second removal surgery could be avoid, thereby health risks, costs and trauma are reduced. In contrast to the metals that are employed in permanent orthopedic applications, corrosion products of Mg have shown to be potentially beneficial to the patient (in low concentration), instead of being either harmful or toxic. Furthermore, Mg it is essential to metabolism and is naturally found in the human body.

Table 1. Some properties of magnesium in comparison with natural bone[15].

Properties	Magnesium	Natural bone
Density (g/cm^3)	1.74-2.0	1.8 - 2.1
Elastic Modulus, E (GPa)	41 - 45	3 - 20
Compressive yield strength (MPa)	65 - 100	130 - 180
Fracture toughness ($MPam^{1/2}$)	15 - 40	3 - 6

The mayor drawback of magnesium in many engineering applications is its low corrosion resistance (especially in electrolytic, aqueous environments). This property has to be considered for biomaterial applications where the *in- vivo* corrosion of the implant involves the formation of a soluble, non-toxic oxide that is excreted in the urine and is harmless. It is expected that magnesium and its alloys be applied as lightweight, degradable, load bearing orthopedic implants, which would remain present in the body and maintain their mechanical integrity over a time scale of approximately 12-18 weeks conferring time to bone healing process to occur and eventually being

replaced by natural tissue. In general, the healing process of bone involves three phases; inflammatory, reparative and remodeling. In the inflammatory phase, the immune system of the body responds against a foreign material. The following phase, the reparative stage, consists on the integration of the implant with new bone and regeneration of tissue takes places. The remodeling phase is the longest phase during the healing process, which involves as minimum 12 weeks, and Mg base implant confronts degradation within this period. Therefore, enhancement of corrosion resistance is needed[16].

Several strategies can be employed to tailor corrosion rate of magnesium. For example, adding alloying elements to the pure Mg or cover the surface with protective coatings. It is important to clarify that the alloying elements as well as the materials used to coat the surface have to be of a non-toxic nature and biocompatible.

A severe consequence of the high chemical reactivity of Mg in physiological environment results in localized corrosion, which leads to a rapid and sooner decreases on mechanical properties of the implant. However, the corrosion behavior strongly depends on the surrounding pH (at high pH a passivation effect is observed, explained later in Section 2.1.1.2). Another consequence is the fast hydrogen gas production, which will bring about a balloon effect, if the absorption through the host tissue is too slow [17]. These important drawbacks make Mg biomedical applications to be limited. The most convenient way to overcome these problems is by applying protective coatings. In this way, it is created a time-dependent barrier to avoid direct contact of Mg with the physiological environment. In addition, tailoring the coating composition and structure can provide accelerated bone regeneration and growth properties [17].

Mg alloy WE43 was developed in an effort to improve the corrosion resistance of pure magnesium, with the addition of small levels of rare elements (RE) (<4%). The first rare-earth alloy was composed of 4wt% yttrium and 3wt% of a rare earth metal mixture consisting of neodymium, cerium and dysprosium (WE43). These elements have acceptable toxicity and are beneficial to enhance the mechanical and corrosion properties [18].

The microstructure of as-cast WE43 alloy consists of a solid solution α-Mg matrix with precipitates of intermetallic phases at grain boundaries and the grain interiors. Irregular precipitates of $Mg_{41}Nd_5$, rectangular particles of MgY phase, particles of $Mg_{24}Y_5$ and longitudinal precipitates of β($Mg_{14}Nd_{12}Y$) [1].The second phase particles such as Mg_{12}(RE) and Y-rich substance have positive potential relative to magnesium matrix, therefore they act as sites for hydrogen evolution in the corrosion process [18]. Moreover, the yttrium element in the Mg WE43 alloy act as impurity remover (H, O, S, Cl, Fe, etc.) by transforming these impurities from solute state substances to intermetallic compounds, which enhances corrosion resistance [18].

2.1.1.2 Corrosion of the metallic implant

A lot of issues may arise with the implant following surgery, but one of the most important is the interaction between the surrounding physiological environment and the surface of the implant itself. This interaction can lead to failure or having and adverse effect on the patient (i.e., rejection of the implant).

Regarding metal implants, the human environment could be considered to be inhospitable: a highly oxygenated saline electrolyte at a pH of around 7.4 and a temperature of 37°C. That is why metallic implants are highly susceptible to corrosion and, therefore, these characteristics have to be taken into account for the material selection or design and fulfill a biological requirement.

Corrosion is the destructive result of chemical reaction between a metal or metal alloy and its environment. Nearly all metallic corrosion processes involve transfer of electronic charge in aqueous solutions. In the electrochemical process, a redox (reduction- oxidation) reaction takes place and an electron transfer/exchange occurs, leading to degradation of the metal. The composite reaction involving charge transfer or exchange of electrons is shown in Figure 1. The metal dissolves by (Eq.1) liberating electrons into the bulk of the metal which migrate to the surface, where they react with H^+ in solution to form H_2 by (Eq. 2)[19].

$$M \rightarrow M^{n+} + ne^- \quad \text{anodic reaction (Eq. 1)}$$

$$nH^+ + ne^- \rightarrow H_2(g) \quad \text{cathodic reaction (Eq. 2)}$$

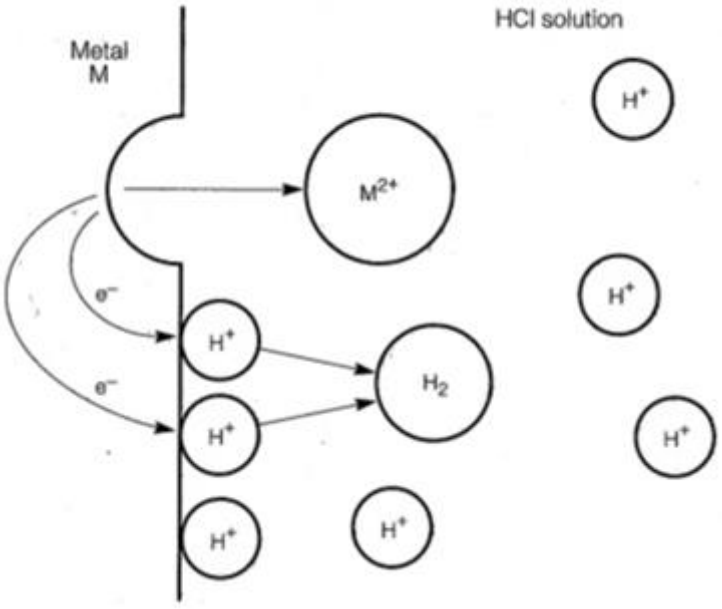

Fig. 1 Schematic diagram of metal M dissolution [19].

Accumulation or defeat of electrons at the surface by Eq.1 or Eq.2 generates a negative or positive potential charge, i.e., cathodic or anodic polarization respectively. In a continuous electrolyte solution the interface will reach a steady state potential, Ecorr, which depends on the ability and rate at which electrons can be exchanged. As the surface potential increases above Ecorr to E, the corrosion rate generally increases. Many metals may exhibit a corrosion resistance behavior, denominated passivity, even though there is a high driving force for corrosion. Passivity is caused by the formation of a thin, protective, hydrated oxide, corrosion-product surface film that acts as a barrier to the anodic dissolution reaction. This passive film is often fragile and its breakdown can result in unpredictable localized forms of corrosion. Figure 2 shows a typical polarization curve of a corroding metal M with a well-defined passivity region. At even higher potentials, the protective film is unstable and the anodic rate increases in the transpassive state[19].

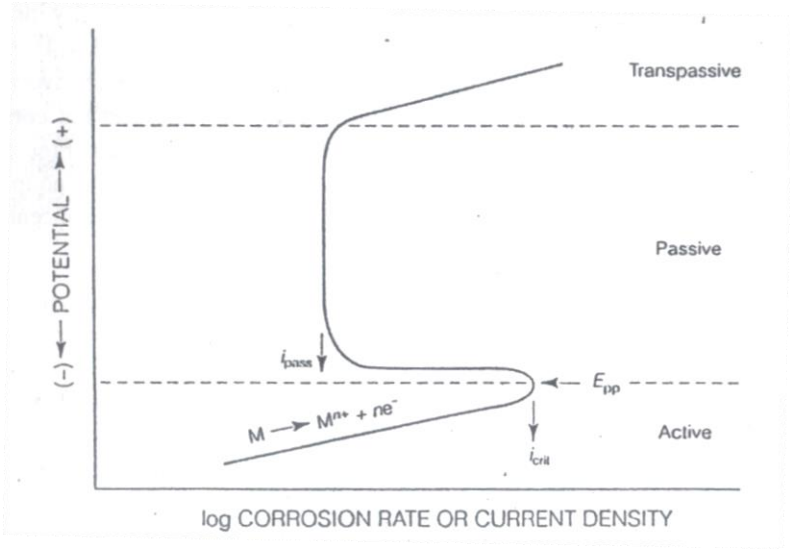

Fig. 2 Typical polarization curves of a metal M in a corrosive medium[19].

The corrosion mechanism for Mg and its alloys when exposed to simulated body fluid (SBF) involves the following process [15][18]:

- Rapid formation of a magnesium hydroxide film (Equation 3). The following film is not compact and possesses a lot of micro-holes, so the matrix is not fully protected. Eventually, the uncovered matrix dissappears and the film thicken.

$$Mg + 2H_2O \rightarrow Mg(OH)_2 + H_2 \text{(Eq.3)}$$

- Agressive ions (such as Cl^-, SO_4^{2-}) transforms the protective film into soluble products.

$$Mg(OH)_2 + 2Cl^- \rightarrow MgCl_2 + 2OH^- \text{(Eq. 4)}$$

Dissolution of the matrix is accelerated due to the presence of Cl^-, which induces pitting corrosion, and due to the solubility of $MgCl_2$.

- Small irregular pieces of Mg alloy peel off from the corroded matrix.

2.2 COATINGS BY DIRECT- CURRENT ELECTROPHORETIC DEPOSITION (DC- EPD)

Electrophoretic deposition (EPD) is a traditional processing method in the ceramic industry, which recently has gained interest both in academia and in the industrial sector for production of new materials. The EPD method provides a very convenient alternative to other techniques such as thermal and plasma spraying, slurry- dipping, sputtering and chemical vapor deposition (CVD). Coatings for electronic, biomedical, optical, catalytic and electrochemical applications as well as structural ceramic coatings for environmental, erosion or oxidation protection are being produced by EPD of nanoparticles [7]. The interest in this technique is the high versatility to be used with different materials (and combination of them) and also because of its cost-effective character, that requires a simple equipment. Besides, EPD not only has a high potential to be used in large scale volume manufacturing and sizes, but also to product a great variety of complex shapes and 3D structures. This results in a broad application range including the production of nanomaterials, biomaterials and ceramic composites.

EPD is a colloidal process in which charged powder particles, that are dispersed or suspended in a suitable liquid, are deposited onto a conductive substrate of opposite charge on application of a direct current electric field (Figure 3). Deposit formation on the electrode occurs via particle coagulation and motion of charged particles results in the accumulation of particles and formation of a homogeneous and rigid deposit at the electrode. This technique offers easy control of thickness and morphology of a deposited film through adjustment of two operational variables: deposition time and applied potential [2][3][5].

A post-EPD processing step, which includes a heat treatment, could be required in order to further densify the deposits and eliminate porosity.

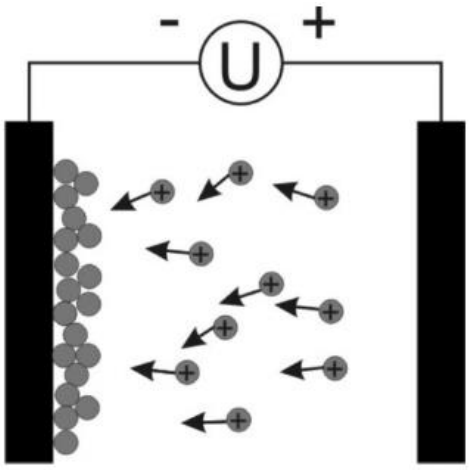

Fig.3 Schematic representation of a traditional EPD cell[5].

The fundamentals on the deposition process results from the Hamaker equation (Eq. 5) [5]:

$$\frac{dY}{dt} = f.\mu.Cs.E.A \qquad \text{(Eq. 5)}$$

Where Y is the deposition field (g), t, the deposition time (s), μ, the electrophoretic mobility (m^2/(V s)), *Cs*, the solids loading in the suspension (g/m^3), E, the electric field strength (V/m), and A the surface area of the electrode (m^2). The factor *f* represents the efficiency with which particles that reach the electrode are deposited.

Factors influencing EPD could be considered in two different groups; parameters related to the suspension and those related to the process (i.e.: physical parameters). In the first group the factors that influence deposition of the material are particle size, dielectric constant of liquid, conductivity and viscosity of suspension, zeta potential and stability of suspension. Considering these variables would result in avoidance of agglomeration and flocculation of particles, poor conductivity to allow deposition, etc. In the second group appears the deposition time, the applied voltage, concentration of solid in suspension and conductivity of substrate. In terms of the deposition time, it was found that the deposition rate for an applied field is decreased with increasing time because of the formation of an insulating layer of ceramic particles on the electrode surface. Normally, the amount of deposit increases with increase on the applied potential, although the quality of the coating can suffer packing disarranges. Considering the concentration of solid particles, especially in multi-component EPD, if the volume fraction of solid is low, the particles can deposit at rates proportional to their individual electrophoretic mobility. Finally, regarding conductivity and uniformity of the substrate electrode, this is an important parameter that affects the quality of deposition of the film. Less conductive electrodes surface could not only create un-uniform coatings, but also the deposition would be slower.

The solvents used for EPD are either organic solvents or water. The use of an aqueous system presents higher advantages compared to organic solvents since they need much lower voltage to be applied (water has a greater dielectric constant which allows the particles to be easily charged) and the environmental and costs problems associated with organics are avoided. However, the use of water-based suspensions causes some disadvantages in electrophoretic processes. Electrolysis of water occurs at low voltages, producing an electrochemical reaction in the electrodes when current is passed through. In this way, gas evolution at the electrodes cannot be avoided at field strengths high enough to give reasonable short deposit times. The later cause bubbles to be trapped within the deposit.

2.3 BIOCOMPATIBLE MATERIALS

Historically, the function of biomaterials has been to replace diseased or damaged tissues. First generation biomaterials (bioinert materials), such as metals, alumina, zirconia, polyethylene, etc. were widely used in the past years in bone tissue replacements with average lifetime of 15 years. Bone strength decrease at about the age of 50 combined with the increase of human life expectancy to about 80 years, made the lifetime of these prosthesis too short, leading to another surgical intervention to replace them. Two reasons cause the shortening of the bioinert implants lifetime and, therefore, their failure: The lack of a biological bond between the implant and the host tissue, which in time leads to wearing and deterioration of the implant, and the weakening of healthy bone due to stress shielding (mismatch on the mechanical properties of the bone and the prosthesis) [22].

In order to overcome these issues that confer great disadvantages to bioinert materials, second generation biomaterials were developed: bioactive glasses. Tissue regeneration and repair using the gene activation properties of Bioglass® constitute the third generation materials.

2.3.1 Bioactive glass

Bioactive glasses were first developed by Hench in 1971. Bioglass® is a biocompatible and degradable material consisting in a silica network as base material that is mixed with other components such as calcium, phosphate and sodium oxides to stimulate bone healing and regeneration. The system of Na_2O-CaO-SiO_2-P_2O_5, high in calcium content and with a composition close to a ternary eutectic in the Na_2O-CaO-Si_2O diagram, is presented in Figure 4. The most common composition is the termed 45S5 and Bioglass®, containing 45% SiO_2, 24.5% Na_2O, 24.5% CaO and 6% P_2O_5 in weight. It was found that by using this material, the body was stimulated to apply its own regenerative capabilities. Therefore, the interest on using this material is that when dissolving in physiological conditions, it activates genes controlling bone regeneration within 48 h [23]. The mechanism for bone bonding is attributed to a hydroxycarbonate apatite (HCA) layer on the surface of the glass. HCA is a ceramic calcium phosphate ($Ca_{10}(PO_4)_6(OH)_2$), whose structure and composition are similar to the mineral phase of bones and teeth, and is thought to integrate (bond) with the host bone. After 40 years of research, no other bioactive glass composition has been found to have better biological properties than the Bioglass 45S5 composition[24].

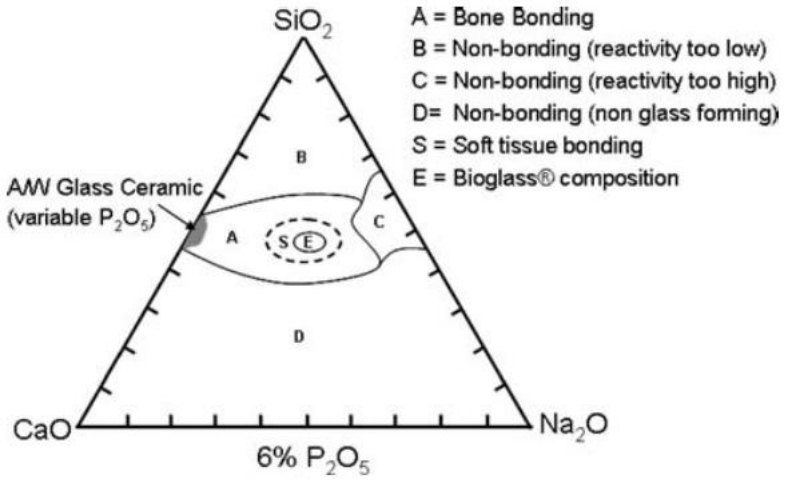

Fig.4 Ternary diagram for bone-bonding[24].

The interest on bioactive glasses in medicine relies on surface modification of implants to enhance bone formation and to bind to surrounding bone tissue [25]. Some drawbacks of bioactive glass coatings are low tensile strength, fatigue resistance and elastic modulus, making it recommendable for orthopedic and dental applications. In this way, it is achieved a synergistic effect of bioactivity and mechanical strength. Mechanical stability of the interface between the coating and substrate has to be taken into account and in order to improve this property, the development of an organic-inorganic composite by dispersing the glass particles within a polymer matrix have shown that is desirable and beneficial [26]. With the addition of the polymer, degradation of Bioglass® can be controlled and the poor adhesion strength of the ceramic particles to the metallic implant can be improved [25].

2.3.1.1 Mechanism of HCA layer formation on bioactive glasses

The hydroxycarbonate apatite (HCA) layer forms following dissolution of the bioactive glass, which causes variation of the chemical composition and of the pH of the solution. This consequences provides surface cites and a pH conducive to HCA nucleation. There are five stages for HCA formation in body fluid *in vivo* or in SBF *in vitro* [27][24]*:*

1. Rapid cation exchange of Na^+ and/or Ca^{2+} with H^+ from solution, creating silanol bonds (Si-OH) on the glass surface:

$$Si\text{-}O^-Na^+ + H^+ + OH^- \rightarrow Si\text{-}OH^+ + Na^+(aq) + OH^-$$

The pH of the solution increases and a silica-rich (cation-depleted) region forms near the glass surface. If any phosphate in the glass present, is also lost.

2. High local pH leads to attack of silica glass network by OH^-, breaking Si-O-Si bonds. Soluble silica is lost in the form of $Si(OH)_4$ to the solution, leaving more Si-OH (silanols) at the glass-solution interface:

$$Si\text{-}O\text{-}Si + H_2O \rightarrow Si\text{-}OH + OH\text{-}Si$$

3. Condensation of Si-OH groups near the glass surface: repolymerization of the silica-rich layer.
4. Migration of Ca^{2+} and PO_4^{3-} groups to the surface through the silica-rich layer and from the solution, forming a film rich in amorphous $CaO\text{-}P_2O_5$ on the silica-rich layer.
5. Incorporation of hydroxyls and carbonate from solution and crystallization of the $CaO\text{-}P_2O_5$film to HCA.

The rate of HCA formation and bone bonding is highly dependent on the glass composition. Basically, lower silica content results in a higher dissolution rate because the network is less interconnected and therefore, the stages listed above are prone to happen faster. Other factors that influence the bioactivity behavior is the activation energy of silica dissolution in the glass, the silica content and which cations modify the glass structure.

The *in vivo* sequence for bone tissue formation continues as the following:

6. Adsorption of biological moieties and growth factors on the HCA layer.
7. Action of macrophages.
8. Attachment of stem cells.
9. Differentiation of stem cells.
10. Generation of matrix.
11. Crystallization of matrix.
12. Proliferation and growth of bone.

Therefore, through this twelve stages bioactive glass bonds to bone, is gradually absorbed and replaced by new tissue.

2.3.2 Calcium-Phosphates

Calcium phosphates (CaP) naturally occur in biological structures like teeth and bone. Basically, bone consists of an inorganic component of biological apatites (CaP) and an organic component consisting primarily of collagen and water. Similarities in properties of natural CaP with synthetic hydroxyapatite made them to be used as coatings for protection against wear corrosion and increased biocompability in orthopedic devices [14].

2.3.3 Silica nanoparticles

Silica nanoparticles have been lately having a prominent position in scientific research, because of their easy method of preparation and their wide uses in various industrial applications, such as catalysis, pigments, pharmacy, electronic and thin film substrates, electronic and thermal insulators, and humidity sensors. The quality of some of these products depends highly on the size and size distribution of these particles [28].

Silica on *in vitro* conditions displays activity on bone – mineralizing cells. Also, silica is beneficial to bone and connective tissue's health. Two properties of silica include inducing biomineralization and acceleration proliferation of bone cells and their precursors. Both properties are intended to be achieved for bone tissue substitute materials [29].

Silica particles affect the proliferation of bone marrow stem cells (BMSC) and their efficiency of producing collagen depending on the release rate of silica from the micro particles. Dissolved silica molecules cause an increase in the production of collagen, while non- dissolving particles seem to enhance the proliferation of bone marrow stromal cells. Proliferation of BMSCs and their efficiency at producing extracellular matrix (ECM) are two key components of bone defect healing. This effect, however, is mediated by specialized cells that ingest micro-scale particles of silica making it a challenge to design proliferation enhancing silica based biomaterials [27].

The synthesis of the spherical and monodispersed silica nanoparticles is based on the hydrolysis of tetraethyl orthosilicate (TEOS) in ethanol medium in the presence of ammonium hydroxide (catalyst). In this sol-gel process two main types of reactions are involved [28]:

- Silanol groups are formed by hydrolysis (Eq.6)
- Siloxane bridges are formed by a condensation polymerization reaction (Eq. 7)

$$Si\text{-}(OR)_4 + H_2O \rightarrow\leftarrow Si\text{-}(OH)_4 + 4R\text{-}OH \qquad \text{Hydrolysis (Eq.6)}$$

$$2Si\text{-}(OH)_4 \rightarrow 2(Si\text{-}O\text{-}Si) + 4H_2O \qquad \text{Condensation (Eq.7)}$$

The main parameters that have to be taken into account on this process, due to affects the particle size and size distribution of silica nanoparticles, are concentration of TEOS, ammonia, water, the alcohol effect and the temperature.

2.3.4 PHBV

Poly (3-hydroxybutyrate-co-3-hydroxyvalerate), commonly denominated PHBV, is a biocompatible, non-toxic and a biodegradable copolymer.

Ceramic scaffolds, such as bioactive glasses scaffolds used in biomedical applications, present low mechanical strength and low fracture toughness. The addition of PHBV particulates to

the surface has been shown to be beneficial and to enhance the mechanical properties of the ceramic matrix. Moreover, this copolymer finds its application in controlled drug release due to their degradation properties, which can be tailored [30].

2.3.5 Chitosan

Natural polymers are promising candidates for biomedical applications because of their similarities with the extracellular matrix, good biological performance and their controlled degradation behavior. Among various natural polymers, polysaccharides have acceptable hemocompability and they are widely found in nature. Chitosan is a natural cationic polysaccharide produced by the deacetylation of chitin, which is the structural element in the exoskeleton of crustaceans and cell walls of fungi. The relevance and use of this material as a biomaterial relies on properties such as antimicrobial activity, chemical stability, biocompability, ability to promote cell adhesion and to chelate metal ions, advanced mechanical properties and excellent film forming ability [8,10]. Its degradation products are non-toxic, non-antigenic, non-immunogenic and non-carcinogenic [31]. Furthermore, chitosan acts as an effective binder, providing adhesion of the particles to the substrate surface and prevents cracking [3]. The molecular structure of chitosan can be seen in Figure 5.

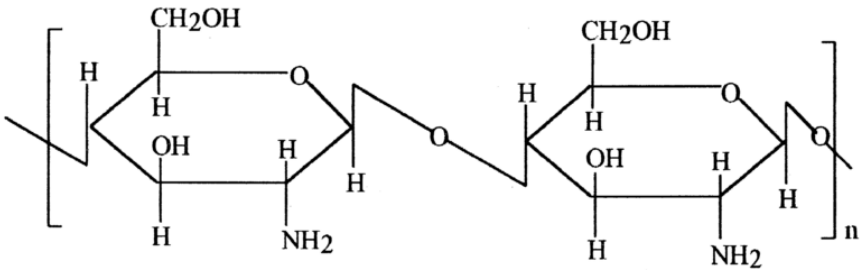

Fig. 5 Chitosan molecular structure[32].

In an aqueous solution, chitosan macromolecules are protonated to form polycations. During the EPD process, electrolysis of water increases the local pH at the cathode. Consequently, the protonated amine-groups of the polymer lose their charge in the high pH region to form an insoluble deposit. The silica – based particles are positively charged in acidic aqueous suspensions, and during the EPD process they move towards the cathode and deposit by coagulation. When a mixture of chitosan and the silica-based particles in an aqueous suspension is prepared, the co-deposition mechanism is governed by the interaction of the chitosan and the particles. The different mechanisms for the chitosan and the particles in the suspension lead to dissimilar deposition rates. Previous studies have shown that the dissolution of the particles increases the pH and conductivity of the suspension, which results in a lower deposition rate of the polymer [3][7].

2.3.6 Polyvinyl alcohol (PVA)

Polyvinyl alcohol (PVA) is a synthetic and water soluble hydrophilic polymer, which has been widely used in pharmaceutical and biomedical application for its acceptable mechanical properties, biocompability, low toxicity and low cost [20].

PVA is a weak polyelectrolyte which is positively charged in acidic solutions. An application on the biomaterials field involves its use for the charging and electrosteric stabilization of EPD suspensions. Moreover, other innovative applications relate PVA-based hydrogels for encapsulation of biomolecules and the combination of PVA with other biopolymers for controlled drug release[25].

2.4 CHARACTERIZATION TECHNIQUES

Typically, the bulk properties of Mg regulates the mechanical integrity of the implant, but the surface properties play important roles in various physico-chemical processes such as interaction with body fluids, adhesion of biomolecules and cells to the metallic implant, which initiates the corrosion process. Therefore, surface characterization must be carried out.

In this work, it were performed different characterization techniques for materials such as optic and scanning electron microscopy, contact angle, techniques based on x-ray (XRD), infrared (FTIR) and Raman spectroscopy, mechanical as roughness test and tape test, and electrochemical test such as potentiodynamic polarization curves and electrochemical impedance spectroscopy.

2.4.1 Roughness test

Rough implant surfaces have shown, through different studies in the biomedicine field , that have a positively influence in healing process by promoting favorable cellular responses and cell surface interactions [13].That is the reason why surface topography is an important factor to take into account. The roughness characterization can be carried out with a roughness gauge, a device with a diamond tip, that when passing it through a certain surface length is capable of amplify the peaks and valleys proper of the surface topography that human eye cannot detect, and quantify them with different parameters. In practice, the most used parameter to register roughness is the arithmetical average roughness Ra, defined by the arithmetical deviations of the roughness profile in relation with the middle line:

$$R_a = \frac{I}{L} = \int_0^L |Y(x)|.\,dx \qquad \text{(Eq.8)}$$

2.4.2 Fourier Transformed Infrared (FTIR)

Fourier Transformed Infrared (FTIR) is the preferred method of infrared spectroscopy. This non-destructive characterization technique is based on irradiating a sample with IR radiation. Some of the radiation is absorbed by the sample and some passes through (is transmitted). The resulting

signal at the detector consists on a spectrum representing a molecular 'fingerprint' of the sample. In order to convert the raw data into the actual signal a Fourier transform is required. The usefulness of infrared spectrum arises because different chemical structures produce different spectral fingerprints.

There are different sampling techniques depending on if the detected signal comes from transmission or reflection data and each of them have different weaknesses and advantages. Among the wide range of application of this device, the spectrometer can provide information as[33]:

- Identification of an unknown solid, liquid or gas.
- Quantitative information, such as additives or contaminants.
- Kinetic information through the growth or decay of infrared absorptions.

2.4.3 Raman spectroscopy

Raman spectroscopy is a versatile, rapid and non - destructive characterization technique. It is based on the principle of the Raman Effect, i.e., the change in wavelength of light that occurs when a light beam is deflected by molecules. It can be used for both qualitative as well as quantitative purpose.

In Raman spectroscopy, the sample is illuminated with a monochromatic laser beam which interacts with the molecules of the sample and originates a scattered light. In most of the cases, the interaction between the photons of the monochromatic beam (with energy proportional to frequency) and the molecules produces an elastic encounter. This means, the photons are scattered with the same energy and frequency as the incident radiation and constitutes the Rayleigh scattering. However, in other cases, the scattered radiation has a frequency different than that of the light beam (inelastic scattering) and is used to construct a Raman spectrum.

A Raman spectrum is presented as intensity- versus- wavelength shift and can be recorded over a range of 4000-10 cm^{-1}. Nevertheless, vibration modes of organic molecules occur in the range of 4000 – 400 cm^{-1}. A Raman spectrum is simpler than their infrared counterparts because in this technique, combination and difference bands are rare, constituting a fingerprint on a molecular level[34]. Raman and FTIR are complementary techniques because while FTIR is strong at identifying functional groups, Raman spectroscopy is well- suited to giving information about molecular backbones. Besides, molecular vibrations that are weak infrared absorbers are often strong Raman scatters, and also applies vice-versa [22].

2.4.4 Electrochemical tests

Evaluating the behavior of the biomaterials in conditions similar to that of the physiological environment is fundamental. The aim of performing corrosion tests could be one or more of the

followings; determine the protective characteristics of a coating, determine probable service life of the implant, evaluate new materials, study corrosion mechanisms, determine the best material for a specific application.

2.4.4.1 Electrochemical Impedance Spectroscopy

Electrochemical impedance spectroscopy (EIS) is a non-destructive technique based on the response of corroding electrodes to small-amplitude alternating potential signals of widely varying frequency. Through this technique can be determined a number of fundamentals parameters relating to electrochemical kinetics.

The time-dependent current response I(t) of an electrode surface to an alternating potential V(t) can be expressed as an angular frequency (ω) dependent impedance Z(ω) [19]:

$$Z(\omega) = V(t)/I(t) \quad \text{(Eq. 9)}$$

Where,

$V(t) = Vo \sin \omega t$,

$I(t) = Io \sin (\omega t + \theta)$,

θ= phase angle between V(t) and I(t).

Various processes at the surface absorb electrical energy at discrete frequencies, causing a time lag and a measurable phase angle, θ, between the excitation (applied voltage) and the response (current).

Impedance, Z(ω), can be expressed in terms of real, Z'(ω), and imaginary, Z''(ω), components in the way: $Z(\omega)=Z'(\omega) + Z''(\omega)$ and representation of the data points are suggested to be in Nyquist plots of Z''(ω) as a function of Z'(ω) or in Bode plots of $\log|Z|$ and $\log\theta$ vs. frequency *f* (Hz). A real response is in phase with the excitation (resistive component) while the imaginary response is not in phase (inductive and capacitive component). Nyquist and Bode plots are shown schematically in Figure 6.

Electrochemical responses in a physiological environment of a metallic material can be interpreted as an electric circuit and different schematic models can be used to represent the corroding phenomena. Figure7 shows a possible representation.

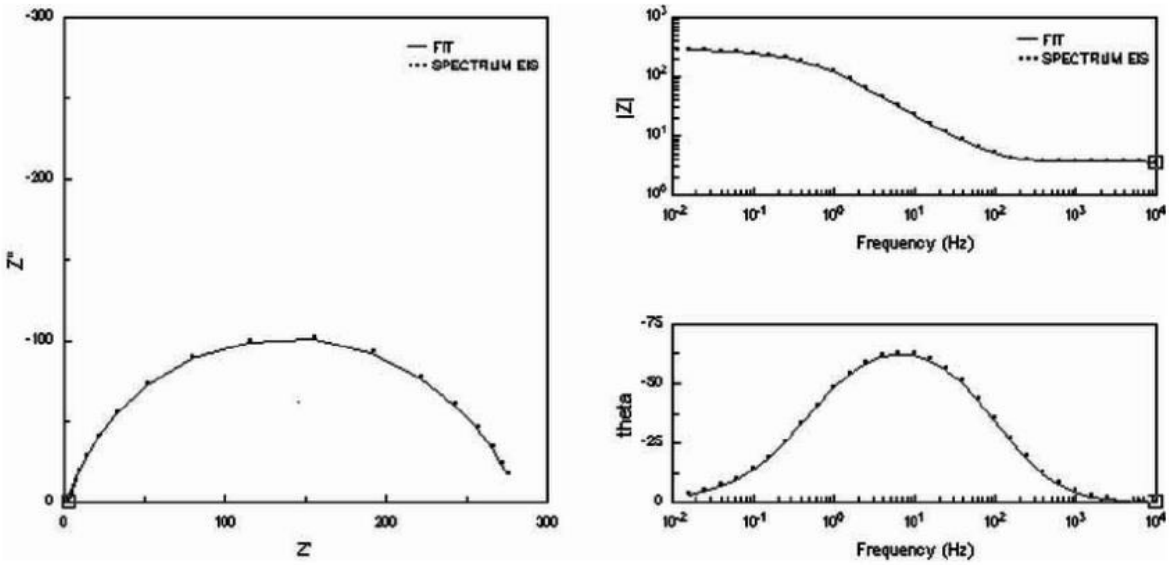

Fig. 6 Schematic representation of Nyquist (left) and Bode (right) plots.

The Nyquist plot shows a semicircle, with increasing frequency in a counterclockwise direction. At a very high frequency, the imaginary component disappears and leaves only the solution resistance R_Ω. As well, at very low frequency that tendency is observed, but now, it leaves the sum of R_Ω and the polarization resistance (R_p). On the other side, a Bode plot gives analogous results with the difference that at intermediate frequencies, the capacitance plots linear with a slope of -1 and maximum phase angle, θ.

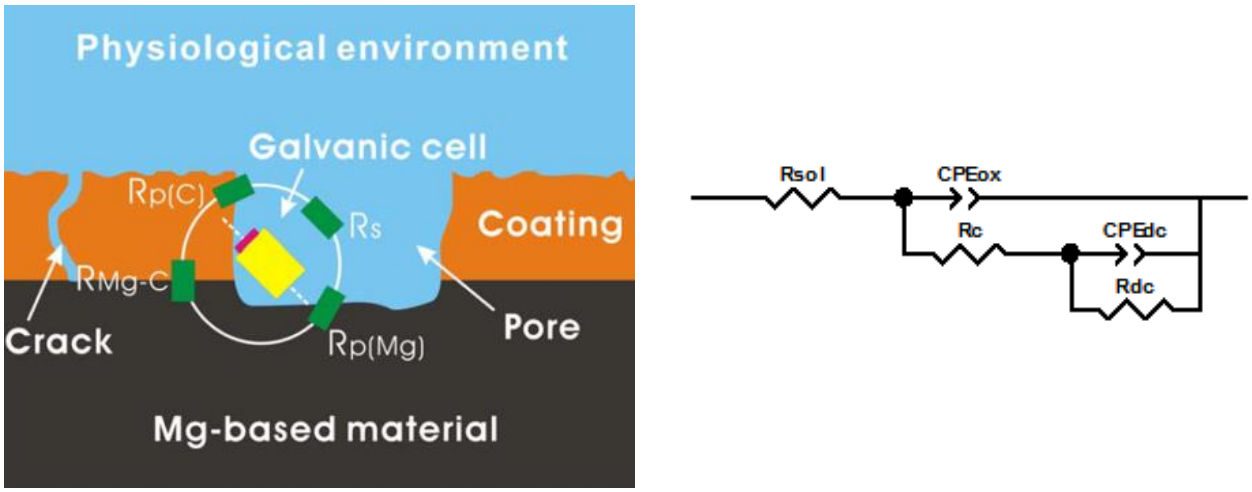

Fig. 7 Schematic diagram showing corroding mechanism of coatings in Mg based materials (left) and the equivalent circuit (right)[17].

2.4.4.2 Potentiodynamic polarization curves

Potentiodynamic polarization is a technique where the potential of the electrode is varied at a controlled rate by application of a current through the electrolyte. This method, which is widely

used in corrosion testing, is a technique that subject the metal under extremes conditions in which generally it will not be exposed during its useful life. However, it is an indicator of possible reactions on *in vivo* conditions. Figure 2, previously presented in Section 2.1.1.2, shows a typical polarization anodic curve for a metal M. This is a destructive technique to simulate and evaluate corrosion.

The chemical transformations which experiment a corroding metal are represented by redox semi reactions and in the case of equilibrium, the oxidation rate is equal to the reduction rate. When one of the redox semi reactions rate is greater than the other one, the equilibrium state is lost and a net current through the metal-medium interface occurs. The metal tends to donate electrons and the medium to accept them, which increases the oxidation rate and consequently, the E_{corr} shifts to more positive values.

Potentiodynamic techniques require that the corrosion potential be stable and unchanging during the measurement. Otherwise, the applied overvoltage and current vary by an unknown amount as the background corrosion potential changes during the test. Besides, the scan must be slowly enough to ensure steady state behavior [19].

3 OBJECTIVES

The general objective of the present final project consisted on generate and characterize a multi-layer, biocompatible and biodegradable coating for the Mg WE43 alloy (4%Y-2%Nd-3.4%Re) through DC- EPD (Direct Current - Electrophoretic Deposition), with the aim of reducing and controlling the substrate corrosion rate and augment the initial bioactivity.

The particular objectives consisted on:

- Synthetize PHBV particles by the emulsion-evaporation method and the silica particles by sol-gel. Analyze its morphology, distribution and particle size through SEM observation.
- Prepare the suspensions with the desired composition for the coatings deposition, substrate preparation (geometry and surface), etc.
- Obtain the different coating systems based in chitosan through EPD. Optimization of the involved parameters (deposition time, applied voltage and composition of the suspension) and selection of the final multi-layer system coating.
- Characterize the surface of the final multi-layer system coating in terms of surface bioactivity and electrochemical behavior.

4 Materials and Methods

4.1 Samples Preparation

4.1.1 Substrate

Mg alloy WE43 was purchased from Helmholz-Zentrum Geesthacht-Magnesium Innovation Center. Chemical composition of the material is presented in Table 2. The samples were obtained by cutting long bars of material every 5 mm width, by use of Struers Secotom-10. The diameter of the bars was 10 mm. After obtaining the desired final shape (Figure 8), preparation of the surface consisted in grinding with SiC grit paper until an equivalent grain size of 5µm. The grinding process was made immediately before deposition of the coating in order to avoid corrosion of the sample, which may influence the deposition character.

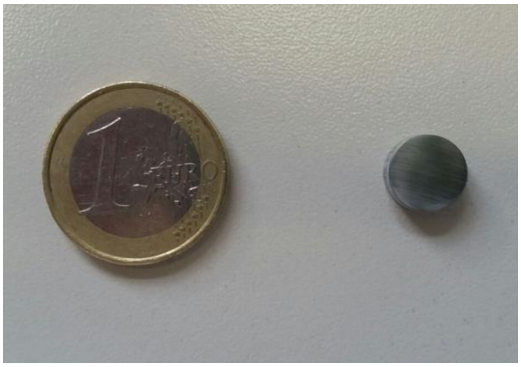

Fig.8. Final sample size and shape after cutting.

Table 2. Chemical composition of the Mg alloy WE43 (% mass)[35].

Mg	Y	Nd	Re	Zr	Mn	Cu	Ni	Zn
89.815	4.0	2.0	3.4	0.4	0.15	0.03	0.005	0.2

4.1.2 PHBV microspheres synthesis

An emulsion evaporation method was used to prepare the PHBV microspheres, taking as a reference the work presented by Li *et al*[30]. The first solution was a 2% w/v aqueous polyvinyl alcohol (PVA) solution mixed at 80°C during 1 hour. At the same time, a second solution of 3%w/v dichloromethane PHBV was mixed at room temperature and during 1 hour. While 150 ml of the aqueous PVA solution were emulsified at 7000 rpm using a homogenizer (T18, IKA, Germany), was added 6 ml of the dichloromethane PHBV solution and emulsified in this way for 3 minutes. After this, the resultant was stirred for 3 hours at room temperature. The samples were 3 times centrifuged (Centrifuge 5430 R, Eppendorf, Germany) for 4 minutes at 5000 rpm and another one

more time centrifuged with deionized water. In order to eliminate the remaining water, the samples were freeze dried in a freeze dryer (Alpha 1-2 LDplus, Martin Christ, Germany) during 17 hours. The microspheres were stored in plastic holders until further use.

4.1.3 Silica nanoparticles synthesis

The reagents used in the synthesis of the silica particles were tetraethyl orthosilicate (TEOS), ammonia and ethanol.

Silica particles were produced by a sol-gel process according to Zahng *et al*[36]. Solutions I and II were prepared separately, with the compositions presented in Table 3. Solution II was added quickly into solution I in a Vicker flask under constant stirring at room temperature during 2 h. After, the solution was divided into two plastic tubes, filled with ethanol and centrifuged. The samples were 3 times centrifuged at 5000 rpm for approximately 2 minutes. After each centrifugation process, the solvent was decanted and the particles were re-dispersed with the help of an ultrasonic bath. An extra centrifugation process was required to eliminate the most amounts of solvent as possible, but this time with deionized water. In order to eliminate the remaining water, the samples were freeze dried for 24 hours.

Table 3. Amounts of components of solutions I and II for the silica particles synthesis.

Solution I		Solution II	
Ethanol (ml)	Ammonia solution (ml)	Ethanol (ml)	TEOS (ml)
46	10	4	1

4.1.4 Suspensions

Different suspensions with varied chemistry or concentration of the components were used during this work to obtain the coatings.

Bioactive glass powder with nominal composition 45% SiO_2, 24.5% Na_2O, 24.5% CaO and 6% P_2O_5 (commercial particle size of 2µm) were purchased from Schott. Chitosan (degree of deacetylation of 75-85%), acetic acid (purity ≥99%), were obtained from Sigma-Aldrich. Ethanol (purity≥99%) was acquired from Emsure. Silica particles were fabricated according to the method described in Section 5.1.3.

Table 4 presents the nomenclature to denominate the suspensions, which will be used from now on.

Table 4. Nomenclature for the different suspensions.

Nomenclature	Suspension
CS-Silica	Chitosan – Silica nanoparticles[1g/L]
PVA-CS-Silica	PVA – Chitosan- Silica nanoparticles[0.8g/L]
CS-BG	Chitosan - Bioglass®

4.1.4.1 Suspension CS-Silica

The suspension CS-Silica used in this work consisted on 1g/L of silica particles and 0.5 g/L chitosan in a solution of 1% vol. acetic acid, 20 %vol. deionized water and 79% vol. ethanol. Chitosan was dissolved in acetic acid and deionized water. After, the solution was magnetically stirred to achieve and adequate dispersion of the components, filled with ethanol and it was left stand for 24 h. Finally, once the silica particles were incorporated, the solution was magnetically stirred for 5 min and sonicated (Bandelin sonorex, Berlin, Germany) during 50 min.

4.1.4.2 Suspension PVA-CS-Silica

Preparation method of suspension PVA-CS-Silica consisted on 1.5 g/L of PVA, 0.5 g/L chitosan and 0.8 g/L of silica particles in a solution of 1%vol.acetic acid, 20%vol. deionized water and 79%vol. ethanol. PVA was dissolved in deionized water during 2 h at 80°C in a magnetically stirrer. After this, the dissolved PVA in deionized water was left to cool down its temperature, and was added the chitosan with acetic acid while magnetically stirring, filled with ethanol and it was left stand for 24 h. Once the silica was incorporated, the solution was magnetically stirred for 5 min and sonicated during 30 min.

4.1.4.3 Suspension CS-BG

The suspension CS-BG consisted on 1g/L of bioactive glass and 0.5 g/L chitosan in a solution of 1% vol. acetic acid, 20 %vol. deionized water and 79% vol. ethanol. The procedure for the preparation of this suspension is equal as the CS-Silica suspension with the difference that was added the bioactive glass instead of the silica particles. Once the bioactive glass was incorporated, the solution was magnetically stirred for 5 min and sonicated during 50 min.

All of the suspensions were once left stand during 24 h to observe the sedimentation character of the particles. No signs of sedimentation were observed.

4.1.5 Calcium Phosphate pretreatment

The CaP pre-treated samples were acquired from the Chair for Surface Science and Corrosion of the Friedrich- Alexander Universität Erlangen-Nürnberg and produced by Höhlinger *et al*[37]. The procedure to obtain the pretreatment was the following [37]: the Mg WE43 alloy samples were immersed for one hour at 60°C in an aqueous 100 ml suspension containing 0.8 mL H_3PO_4, 250 mg ZnO, 120 mg CaO and 1250 mg $Ca(NO_3)2.4H_2O$ with a pH value between 2.8 and 2. Afterwards, the samples were dried at 80°C for 30 min before they were immersed in a 2 M NaOH solution at the same temperature for 3 h. The alkali heat treatment was done to promote formation of hydroxyapatite. Finally, they were dried again for 30 min at 80°C.

4.2 COATINGS DEPOSITION BY EPD

All of the coatings were produced by Direct Current - Electrophoretic Deposition (DC-EPD). The electrodes used in this work were a plate of stainless steel 316L and the Mg WE43 samples previously cut and grinded, as explained in Section 4.1.1. The stainless steel 316L plates were firstly cleaned with ethanol in an ultrasonic bath and consecutively dried properly and carefully. The electrodes were submerged in a 50 ml suspension with a distance between them of 1 cm, which was always maintained constant. The operational variables on EPD, applied voltage and deposition time, were varied in the range between 15 V-85V and between 20 s-90 s respectively.

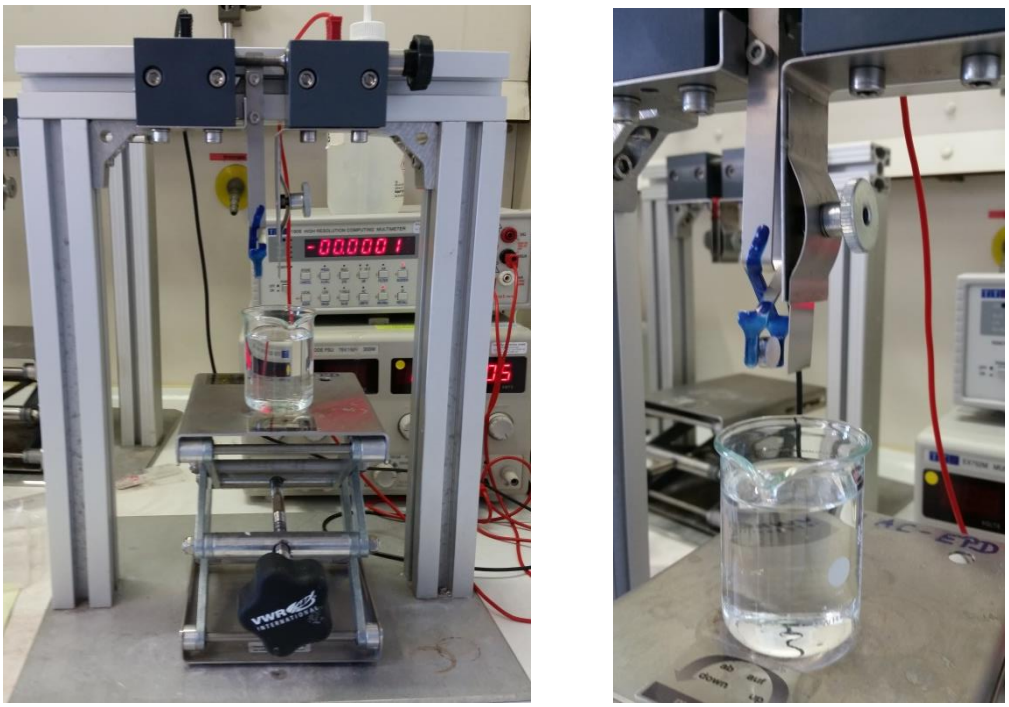

Fig. 9 Electrophoretic deposition equipment and sample holder employed.

The Mg sample holder had to be covered with a non-conductive polymer in order to avoid contact of the metallic holder with the suspension. In this way was avoided the deposition and creation of a coating on the holder instead of on the sample.

4.3 SAMPLE CHARACTERIZATION

4.3.1 Optical microscopy and Scanning Electron Microscopy (SEM)

Optical microscopy (M50, Leica) was used to register the physical appearance of the surface of the substrate the day after the deposition of the coatings, once the samples were dried overnight. Capturing images were obtained by use of Leica Application Suite 3.8.0 software.

The microstructure and morphology of the coatings were also investigated using a scanning electron microscope (SEM, model Auriga, Zeiss) with 1keV electric beam power.

Optical microscopy and SEM were carried out to characterize the surface of the coatings obtained by applying different parameters of deposition or by employing suspensions with varied chemistry and composition. Results of these characterizations allowed to extract conclusions and to select the best coating observed (i.e., the most homogeneous coating, which covers the entire surface of the substrate, and with the less amount of cracks and holes as possible). Further surface and *in-vitro* characterization was only made to the selected coating.

4.3.1 Contact angle

Contact angle measurements were carried out on the samples for the final coating using a DSA30 contact angle measuring instrument (Kruess, Germany) in static mode using deionized water droplets. The bare substrate and the final multi-layer system were characterized to observe the difference in wettability between both surfaces. Reported data were obtained by averaging the results of ten measurements.

4.3.2 Roughness Test

Surface roughness was measured by means of a Taylor-Hobson Surtronic 3+ tester. The software used to analyze the results was TalyMap Gold. Roughness test was made in order to obtain a surface roughness profile and surface quality after deposition of the final coating. The bare alloy was used as reference.

The parameter used for the roughness measure is the average roughness (Ra), defined as the arithmetical average of the superficial profile in relation with the middle line. Four roughness measurements were carried out on the bare sample and on the coated system.

Body-implant interaction and their successful corresponding integration depend strongly on the surface properties. High surface roughness and hydrophilicity are essential to promote cell adhesion and rapid bone formation at the tissue implant interface *in vivo*.

4.3.3 Tape test

The coating adhesion was evaluated by standard tape test using a cross-hatch cutter (Model Elcometer 107) according to the ASTM D3359-B method. This is a tape-peel off test wherein lattice patterns with 11 cuts in two orthogonal directions are made in the coating down to the substrate. Pressure-sensitive tape is applied over the lattice and then removed by pulling it out parallel to the substrate in a single smooth action.

4.4 *IN-VITRO* CHARACTERIZATION

In vitro studies are absolutely important to understand factors that determine the properties of materials under influence of similar conditions to that of human body. Among the techniques used to characterize the surface reaction of the implants immersed in simulated body fluids as a function of time can be found: optical microscopy, SEM, FTIR, Raman spectroscopy and XRD.

4.4.1 Characterization of bare alloy oxides

The bare alloy and the coated sample were immersed in 0.1 M NaCl during 30 min. After immersion, the substrates were rinsed gently with deionized water and left to dry. Characterization of the corrosion products formed during immersion in this electrolyte consisted on optical microscopy and Raman spectroscopy.

4.4.2 Bioactivity test

Carbonate apatite formation on the surface of a biomaterial is thought to be one of the events leading to form a strong chemical bond between the implant and body tissue. In order to characterize a material and determine whether it is bioactive or not when placing it into the human body, immersion in SBF or DMEM has to be done. If hydroxyapatite formation occurs after certain time under immersion in a liquid that simulates human body environment, it does not mean yet this material has a bioactive character. Further *in vivo* characterization must be carried out.

4.4.2.1 Simulated Body Fluid (SBF)

The multi-layer coatings were investigated to their hydroxyapatite forming ability in a simulated body fluid (SBF) with ion concentrations nearly equal to those of human blood plasma.

SBF was prepared according to Kokubo *et al* [38]. The reagents used and their corresponding amounts are listed in Table 5.

Table 5. Amount of reagents for SBF.

Order	Reagent	Purity	Amount (g) for 1LSBF
1	Sodium chloride (NaCl)	100	7.9948
2	Sodium hydrogen carbonate($NaHCO_3$)	100.0	0.3532
3	Potassium chloride(KCl)	99.5	0.2250
4	Di-potassium hydrogen phosphate trihydrate ($K_2HPO_4.3H_2O$)	99.0	0.2310
5	Magnesium chloride hexahydrate($MgCl_2.6H_2O$)	100.5	0.3033
6	1M HCl		39 ml
7	Calcium chloride ($CaCl_2.2H_2O$)	101.0	0.3636
8	sodium sulfate (Na_2SO_4)	99.6	0.0714
9	Tris-hydroxymethyl aminomethane	100.0	6.0568
10	1M HCl		0-5 ml

In order to prepare 1000 ml of SBF, 700 ml of ion-exchanged and distilled water with a stirring bar were put into a 1000 ml plastic Vicker. The water was heated and maintained in 36.5± 1.5°C under continuous stirring. During the whole process it was taken in care that the solution was kept transparent and colorless and that there was no deposit on the surface of the bottle. All the reagents of 1^{st} to 8^{th} order (Table 5) were dissolved one by one in the order given above. Reagents 9^{th} and 10^{th} (Tris and HCl respectively) were added as follows: Little amounts of Tris were added carefully until pH raced to 7.45± 0.01. In that moment, drops of HCl were added to low the pH to 7.42± 0.1. After that, once again was dissolved more Tris until the pH has risen to 7.45± 0.01. This process was repeated until the whole amount of Tris was dissolved and then the pH was finally adjusted with HCl to 7.40 exactly. The Vicker was rinsed with distilled water until filling it at 1000 ml. The SBF solution was maintained in a refrigerator at 5-10°C and used before 30 days after preparation.

The volume of SBF used for each sample was calculated following the Equation 10[38]:

$$V_s=S_a/10 \quad \text{(Eq.10)}$$

Where *Vs* is the volume of SBF (ml) and *Sa* is the apparent surface area of specimen (mm^2).

The samples were immersed in 30 ml of SBF and maintained at 37°C in an incubator (IKA KS 3000 I control) for 2h, 1, 2, 3 and 7 days. Once removed from the incubator, the samples were gently washed with water and left to dry in a desiccator for further examination.

4.4.2.2 pH measurements

The biocompability of a material is a function of the manner in which it alters local tissue physiology. Following of the pH evolution of the coated Mg WE43 alloy from 0 to 7 days of immersion in SBF is an important parameter, which can help to understand the time dependence dissolution of bioactive glasses to create a suitable environment for HA formation to occur.

4.4.3 Fourier Transformed Infrared Spectroscopy (FTIR)

The organic and ionic groups were characterized by FTIR. The spectra were collected using a Nicolet 6700 spectrometer in the range between 4000 and 400 $cm^{-1}$and resolution of 4 cm^{-1}. The final chosen multi-layer system was characterized before and after immersion in SBF during 2h, 1, 2, 3 and 7 days.

4.4.4 Raman spectroscopy

Raman spectroscopy was performed on the samples before and after 7 days of immersion in SBF. The objective was to identify the phases present on the surface of the substrate. The spectra were collected with a confocal Reflex (Renishaw RM 2000, UK). Laser was of 785nm and it was employed 1% and 5% potency to avoid damaging the sample. The wavenumber range was between 300cm^{-1} and 1800 cm^{-1}.

4.4.5 X-Ray Diffraction (XRD)

XRD is one of the most common techniques used in the characterization of materials structure [16].This technique was employed to identify the present crystalline phases of the coated substrates before and after immersion in SBF for 7 days. The samples were characterized using XRD analysis (Philips X'Pert PRO, 40 kV/ 30mA, Cu Kα).Data were collected over the 2theta range from 10° to 80° using a step size 0.01°. Peak identification was carried out with Match! 3 software.

4.4.6 Electrochemical tests

The electrochemical behavior of the coating was investigated in order to test their possible protective properties. For this purpose was used a Zahner Elektrik GmbH setup consisting on a classical three electrode cell with platinum as counter electrode, copper electrode (+0.314 V vs. SHE) as reference electrode and the samples as working electrodes (0.38 cm^2 exposed area). The scanning rate was 1mV/s.

Electrochemical tests were made over bare Mg alloy WE43 samples and over the coated substrates. Preparation of the samples consisted in grinding of the back side of them in order to increase the contact with the working electrode.

All of the electrochemical tests were performed at ambient temperature employing a 0,1M NaCl electrolyte, which is widely used for corrosion studies. Due to verifying reproductively and consistency of the results, three bare alloys and three coated substrates were tested. Working conditions were maintained equally to all tests.

Open circuit polarization was registered during 1800 seconds to achieve stabilization of the corrosion potential. After that, electrochemical impedance spectroscopy and anodic polarization was carried out. The branch of frequencies employed in EIS was from an initial frequency 100000 Hz to a final frequency of 0.010 Hz. The amplitude of the potential was ±10 mV related to the corrosion potential.

5 RESULTS AND DISCUSSION

5.1 COMPARISON BETWEEN PHBV MICROSPHERES AND SILICA PARTICLES

A possible way to increase mechanical properties of coatings is with the addition of particulates reinforcements. Two alternatives were considered: PHBV microspheres and silica particles.

PHBV microspheres were synthesized according to *Li et al* [30]. In Figure 10 can be seen the SEM image of PHBV microspheres obtained after following the procedure mentioned in Section 4.1.2, while for comparison purposes Figure 11 exhibits the SEM image of the microspheres obtained by Li *et al*.

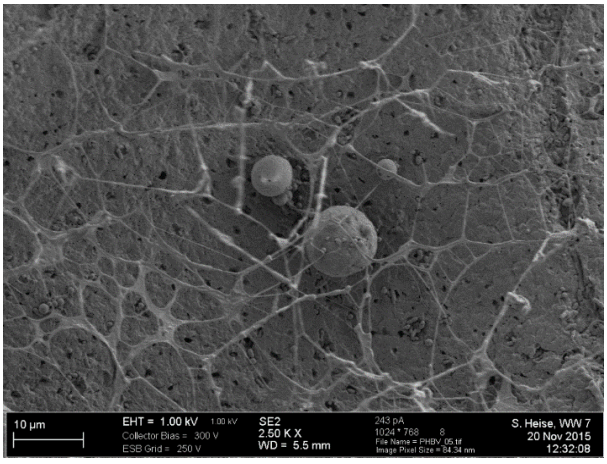

Fig.10 SEM image of the obtained PHBV particles at 2500x.

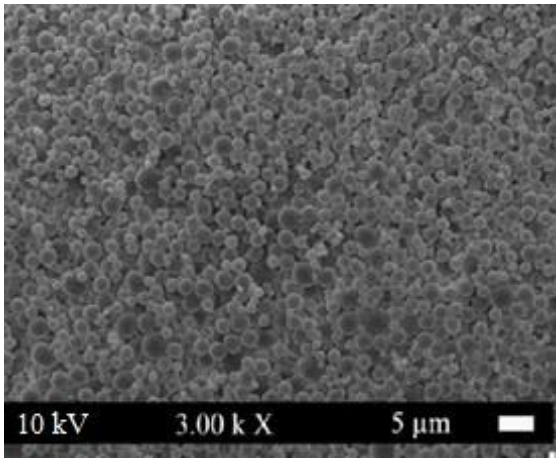

Fig.11 SEM image of the PHBV particles corresponding to Li *et al*[30] at 3000x.

The particles obtained through this technique resulted to be neither uniform nor monodispersed and the amount of them were extremely low. In addition, there was formation of a network that surrounds the spheres and a porous structure underneath. Comparison of the physical appearance of the microspheres between Figure 10 and Figure 11 reveals that they are not alike. The amount of the theoretical particles is greater, exhibit a well monodispersed size and there is no clear formation of a polymer network, in contrast to Figure 10. The procedure published by *Li et al.* was carefully followed but apparently and as the present results showed, no successful PHBV particles were obtained with this synthesis. Due to these reasons and to the carcinogenic potential of dichloromethane[30], which is employed in this synthesis, the synthesis of PHBV particles was discarded.

The other alternative was to synthetize silica particles. Silica particles were prepared according the procedure presented by Zhang *et al* [36] and explained in detail in Section 4.1.3. In Figure 12 the SEM images of the silica particles obtained at different magnifications can be seen. The particles were previously sputtered with gold to avoid charging artifacts during imaging. At lower

magnifications (Fig.12-left) it is observed that this method produces uniform, spherical and monodispersed silica particles. It can also be attended the presence of a little amount of agglomeration. The mean size, obtained through image processing (Image J), resulted to be 160±20 nm.

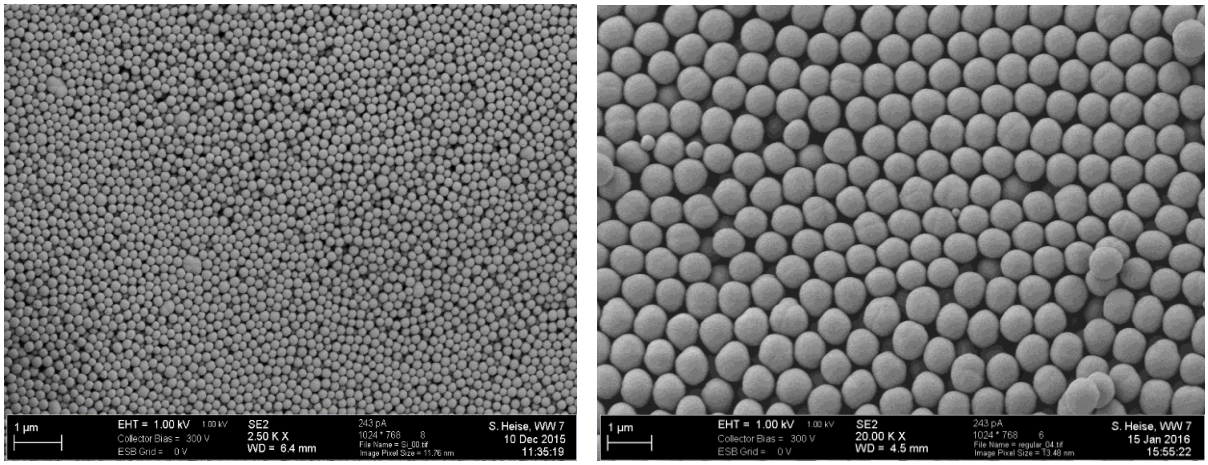

Fig.12 SEM images of the silica particles at 2500x (left) and at 20000x (right).

Differences between PHBV microspheres and silica particles can be easily noticed by comparison of both SEM images (Fig. 10 and Fig. 12, respectively). The proposed method for the synthesis of the silica particles is an easy procedure to obtain high amount, monodispersed and spherical particles. Besides, this process involves non-carcinogenic or hazardous substances, in opposition to the PHBV synthesis method. In addition, silica particles play an important role in the bioactivity and osteogenic potential of Bioglass®. The silanol groups (Si-OH), present in amorphous silica, tend to induce enhanced hydroxyapatite. Previous studies in tibial bone of young rats and mice had shown higher concentration of silica in the active bone mineralization region [8]. For all these reasons, silica particles where selected instead of the PHBV microspheres.

5.2 SELECTION OF MULTI-LAYER COATING SYSTEM

In order to control and modify the corrosion rate of the Mg WE43 alloy and to induce a bioactive behavior for bone regeneration were deposited different monolayer systems over the substrate. The effectiveness of a coating relies, among other characteristics, on obtaining a continuous layer all over the surface. If any hole or any other defect in the coating leaves a superficial area uncovered, the corrosion of the implant would be faster, which is the opposite of what is intended to achieve in the present work. The operational variables involved in DC-EPD (applied voltage and deposition time) were modified to seek, through the trial-and-error method, a coating that covers the entire surface. Criteria for the selection of a suitable coating consisted on determining if the surface was completely covered, was not detached after drying and the amount

of defects were barely observed. This selection was carried out through macroscopic and microscopic analysis.

Following the selection of the best coating obtained (in accordance to the mentioned criteria), it was carried out the surface characterization and also the *in vitro* characterization.

The pursuit of a coating that fulfills the requirements lied to three different multi-layer systems, classified according the composition of the layers.

5.2.1 Silica system

The first suspension used to cover the surface of the Mg WE43 substrate was the suspension CS-Silica (Chitosan-Silica) suspension (See Section 4.1.4.1). To simplify the nomenclature, all of the multi-layer coatings that acquired their first layer by use of this suspension will be denominated as 'silica system' from now on. Figure 13 shows the optical microscopy images of two different samples obtained at different deposition variables. The following images correspond to the best two combinations of parameters after the trial-and-error method.

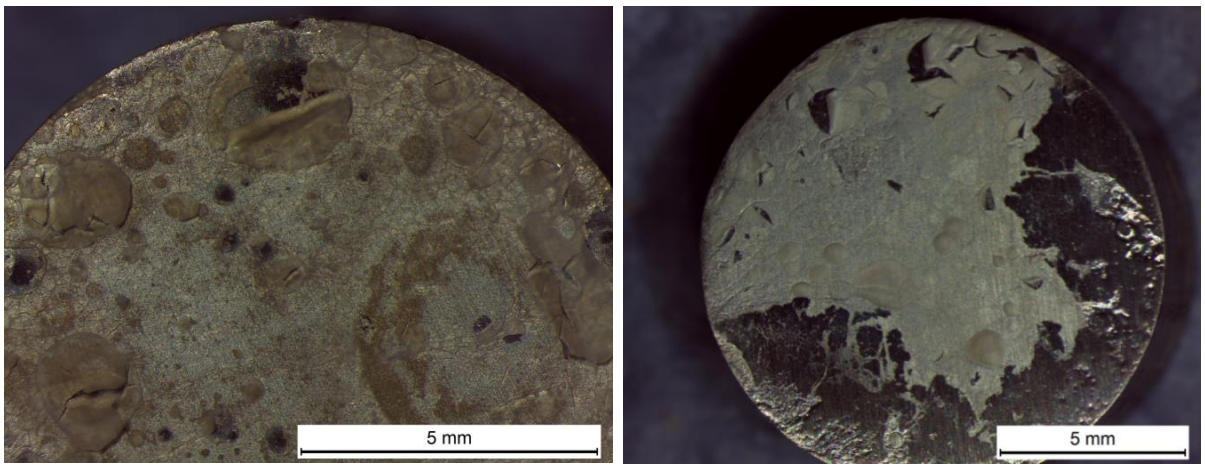

Fig. 13 Optical microscopy of the single layer (CS/Silica particles) coating .Deposition parameters: (left) 70 V during 45seconds; (right) 50 V during 60 seconds.

During drying, the coating densifies and as a result it shrinks, but the substrate typically does not change its dimension. During this process, the coating will develop tensile stress in it and these stresses will be relieved by the formation of cracks and tearing. This later explains the several cracks that can be seen in the image.

Different kind of defects can be observed in both images and among them can be found cracking, uncovered areas, poor adhesion and bubble formation. Comparing the tonality of both coatings to that of the original suspension, the coating of Figure 13 (left) presents darker areas, which could be signs of corrosion due to applied high voltages. Figure 13 (right) shows a not entirely covered surface and there are also holes caused by tearing due to the contraction. Bubbles over the

surface are attributed to the hydrolysis of water and Mg corrosion in the electrolyte. Modification of the operational variables of EPD (applied voltage and deposition time) showed constantly all these kinds of defects, in mayor or lower grade.

A closer examination of the surface with SEM reveals areas where there is no deposition of a material (Figure 14 - right), determined by the clear signs of the parallel grinding lines. In Figure 14-left, are also shown cracks due to contraction and bubbles, possibly formed due to Mg corrosion in the electrophoretic process and due to the hydrogen evolution.

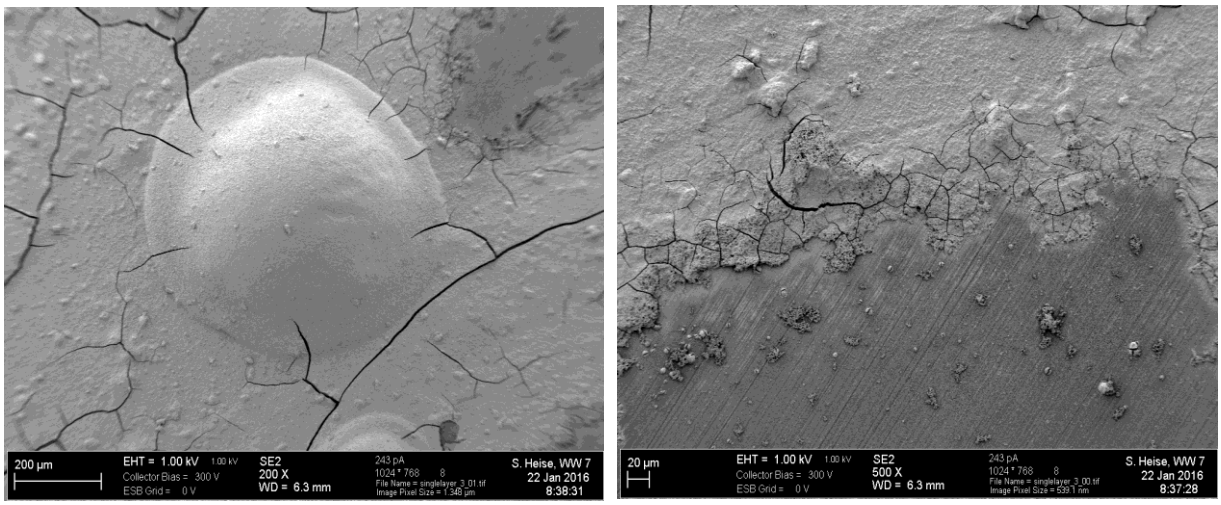

Fig.14 SEM images of the single layer (CS/silica particles) coating showing uncovered areas, cracks and particle agglomeration at (left) 200x and (right) 500x.

None of the cases previously shown, demonstrated to fulfill the macroscopic and microscopic requirements in order to become a suitable coating for the Mg alloy substrate. Therefore, different approaches were carried out in an effort to solve these defects and obtain the desired coating. There were considered different alternatives to overcome these defects: the sample with the best monolayer macro and microscopically observed was selected to be covered with a second layer. The trial-and-error method determined that the best coating obtained with this suspension was with the deposition parameters 35 V and 90 s.

Since the first layer of CS-Silica presented the previously detailed defects, an approach to overcome these defects was to cover the layer with a second layer of CS. By depositing a second layer, the uncovered areas would now be covered and this defect would be overcome. The best combination of parameters for the second layer was 30 V 50s.

Figure 15 presents the SEM images of the substrate after deposition of the second layer. At low magnifications (Figure 15-A) can be seen a quite homogeneous surface, with some particle agglomeration and few cracks. At higher magnifications (Figure 15- B,C) can be seen two delimited zones. The outer zone consists on the first coating, composed of chitosan and the silica particles,

which can be seen in these images. On the other side, the inner area presents several parallel lines, which consisted on the grinding lines of the Mg surface. There are no signs of silica particles in this area, therefore, is concluded that after the electrophoretic deposition of the first coating, an area remained uncovered (the inner zone), which after the second suspension, was covered with chitosan. Even though the second chitosan layer effectively covered the uncovered remaining area from the first deposition, it still presents cracks and adhesion defects.

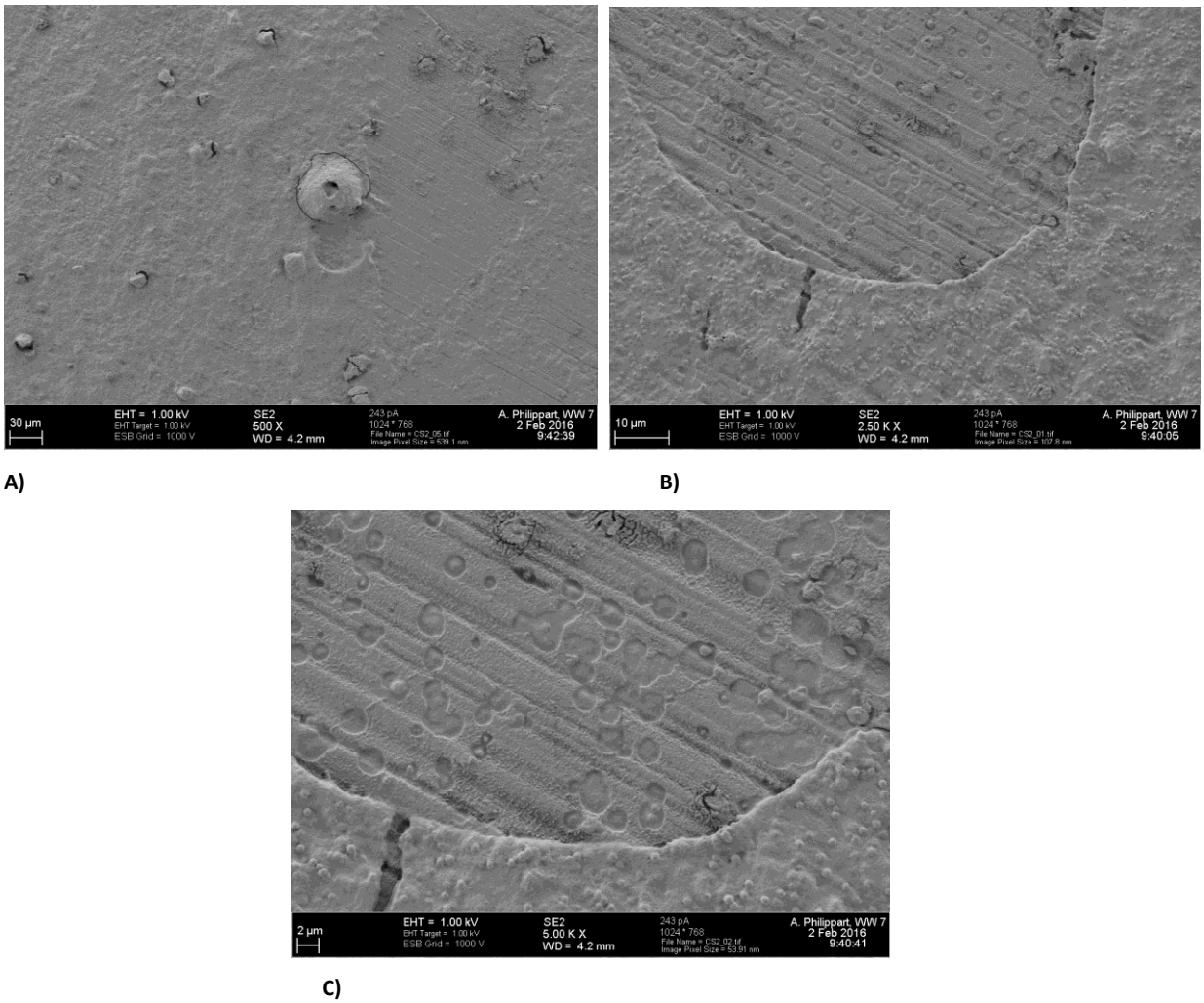

A) **B)**

C)

Fig. 15 SEM images of the multi-layer coated system, containg a first layer of CS-Silica and second layer of CS, at A) 500x B) 2500x C) 5000x. Deposition parameters for the CS solution: 35V 50s.

The other alternative, which was taken into account to cover the defects obtained by the first layer, was to deposit a second coating from the same suspension of CS-Silica. Figure 16 reveals the surface appearance of the resulting multi-layer coating through SEM. In this analyzed area can be easily observed a region which resulted to be uncovered after the first deposition and poorly covered after the second layer deposition.

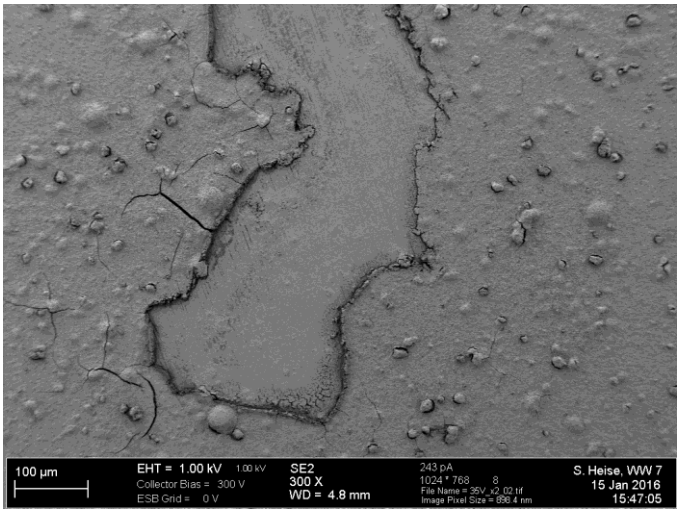

Fig.16 SEM image of the multi-layer coating, formed by deposition of two layers of CS-Silica particles, at 300 x.

In Figure 16 is also revealed the presence of cracks, bubbles and agglomeration of particles. Since by none of these alternatives were obtained a continuous coating, the composition of the first layer was modified.

5.2.2 PVA system

The Cs-Silica system could not provide a suitable coating per se. That is the reason why the chemical composition of the suspension had to be adjusted. A binder (PVA) was added with the aim to enhance the adhesion of the coating to the metallic substrate [20], and the silica particles concentration was decreased. The resulting PVA-CS-Silica suspension (see Section 4.1.4.2) was employed to deposit the first coating. The mono or multi-layer coatings obtained with this suspension will be denominated as 'PVA system' to simplify nomenclature.

As it was previously said, an improvement on the adhesion of the coating to the substrate is expected to occur by reducing the silica concentration in the solution. This is due to a decrease in porosity generated for the silica particles in the chitosan matrix.

Polymer binders are added in EPD processes for different reasons. Binders, like PVA, are used to acquire adherent deposits and crack free surfaces. Moreover, these additives provide steric stabilization to the suspension of the ceramic particles and reduce viscosity of the suspension [39]. The blend of two polymer species, such as PVA and chitosan, have shown in previous studies [40] that the mechanical properties are significatively enhanced. Moreover, previous publications related to PVA coated hydroxyapatite over stainless steel plates determined that addition of the binder does not have a great influence on deposition amount. However, homogeneity and adhesion of the coatings were increased with PVA concentration until 5 wt.% [41].

Figure 17 shows the best mono-layer coating obtained with this suspension (deposition parameters: 40 V 60 s). As can be seen, adhesion and homogeneity, as well as the percentage of covered area, were improved comparing it with the CS-Silica system. Defects, such as cracks due to contraction and bubbles were significantly reduced.

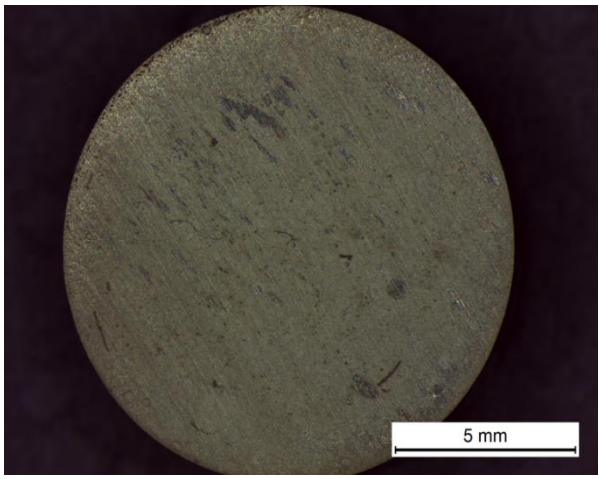

Fig. 17 Optical microscopy of the substrate coated with one layer of PVA-CS-Silica.

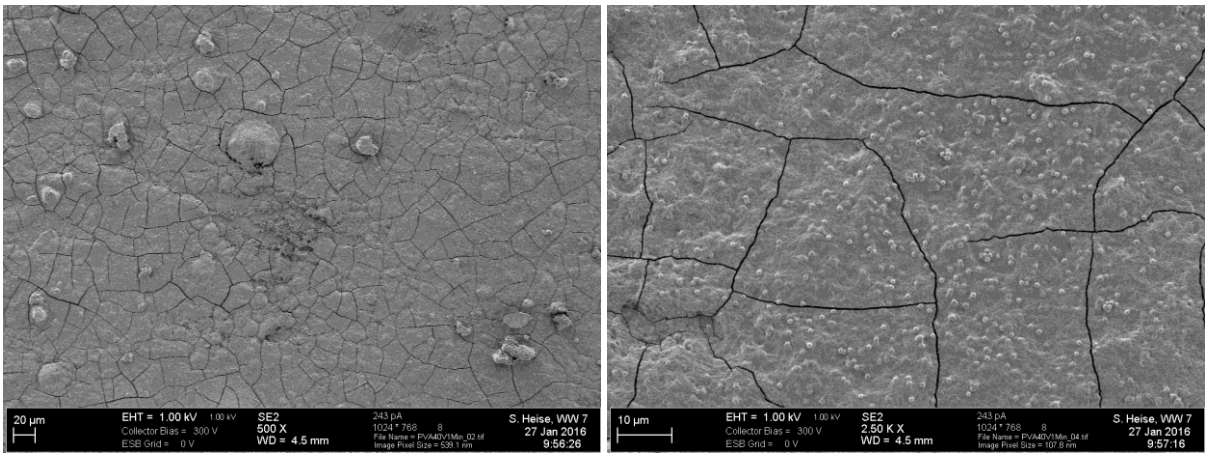

Fig.18 SEM images of the substrate coated with one layer of PVA-CS-Silica at (left) 500x and (right) 2500x.

Figure 18 shows the SEM images corresponding to the substrate observed in Figure 17. At lower magnifications (Fig.18-left) can be seen that the surface is fully cracked; there is agglomeration of material and areas not completely coated. At higher magnifications (Fig.18-right) are observed the chitosan matrix with the embedded silica particles, greater particulates in size which stands for silica agglomerates and an uncovered region. The main defect that appears in this coating is the appearance of cracks, which are distributed over the entire surface of the deposited layer. A possible way to tackle this undesired defect is by applying a second layer.

Due to the results obtained in the previous case, a second layer composed of chitosan was implemented. The later objective was to coat the uncovered areas, formed by the first deposition.

Figure 19 shows the SEM images of the multi-layer system. Even though the amount of fissures and cracks from the first deposition layer where covered, there was the presence of other defects such as bubble formation and tearing of big coating areas. At higher magnification (Fig.19- right) is no longer possible to distinguish the silica particles, and is concluded that the chitosan layer may have been too thick.

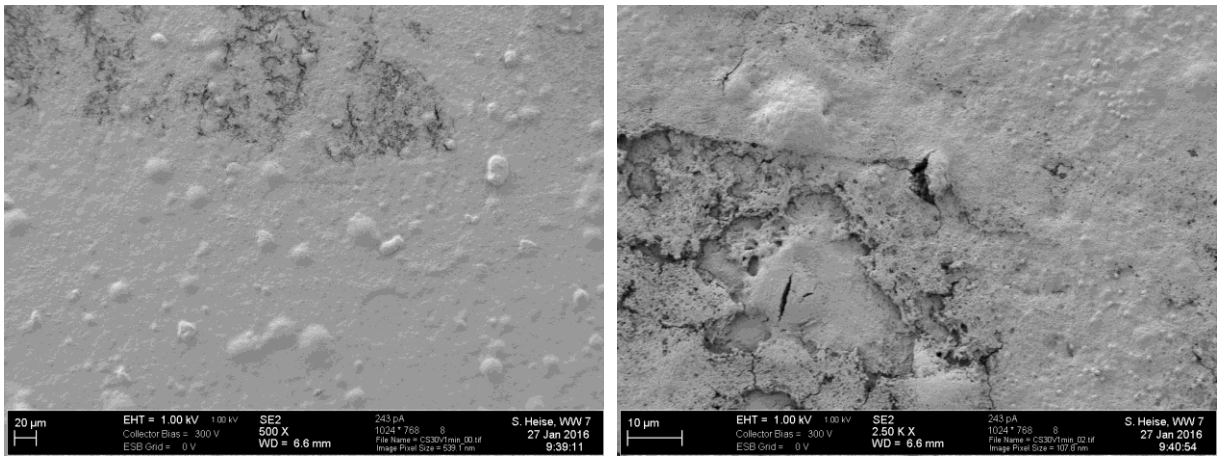

Fig.19 SEM images of the multi-layer coated substrate, constituted by a first layer of PVA-CS-Silica and a second layer of CS, at (left) 500x and (right) 2500x.

Using an aqueous route to prepare these kinds of coatings facilitates the corrosion of Mg surfaces during the electrophoretic deposition of the materials. Substrate dissolution and the H_2 evolution make difficult the deposition of a compact layer. A possible way to tackle this inconvenient is by generating a calcium phosphate pre-treatment to the sample. The aim of an optimum pre-treatment on a metallic exposed surface is to decrease corrosion rate of the substrate, provide good bonding to the surface and with the coating [37].

In Figure 20 can be seen the optical microscopy of the previously CaP pre-treated sample after deposition of the PVA-CS-Silica layer. As it is shown, even though the thickness seems to be greater than in the other cases, there is the appearance of macroscopic peeling, showing bad adhesion to the substrate. The amount of bubbles due to H_2 decomposition was remarkable lower, as expected because of the protection of the substrate with the pre-treatment. Figure 21 shows the SEM image of the coating. The particles distribution was homogeneous, there was the presence of a few agglomerates and there was practically no micro-crack observed. However, the poor adhesion to the substrate observed macroscopically, made this pre-treatment discardable for this present project.

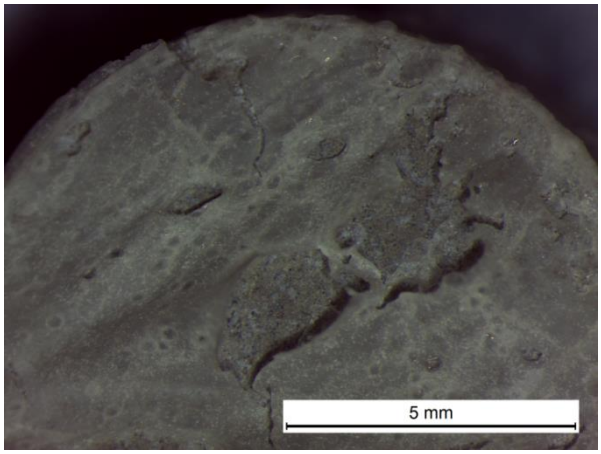

Fig. 20 Optical microscopy of the pretreated sample after deposition of one layer of PVA-CS-Silica.

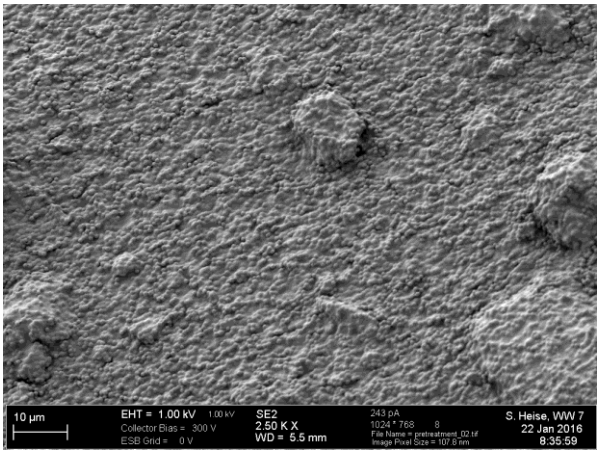

Fig. 21 SEM image of the pretreated sample after deposition of one layer of PVA-CS-Silica at 2500x.

The strategies employed were not efficient to obtain a continuous coating that covers the entire surface of the Mg WE43 sample.

5.2.3 Bioglass system

As it was shown in the previously analyzed systems, several defects were found after deposition of the first and the second coating. Even though different strategies were used to tackle these defects, it was concluded that in these conditions no completely covered surface was obtained and that the pursuit of a totally covered substrate would have to be achieved by making a change in the chemistry of the first layer. Therefore, a bioglass system consisting of a first layer of bioactive glass 45S5 and chitosan was considered.

The best EPD parameters for the first layer onto the Mg WE43 alloy employing the CS-Bioglass® suspension were 50 V during 60 s. It was obtained a homogeneous coating but some remaining areas resulted to be uncovered. Figure 22 presents the SEM micrographs of the best coating obtained, where at low magnifications can be seen the Bioglass® particles distributed on the surface. The particles distribution is not homogeneous; there are some huge agglomerates (Fig. 22-right) and the uncovered areas are revealed by observation of the grinding lines on Mg.

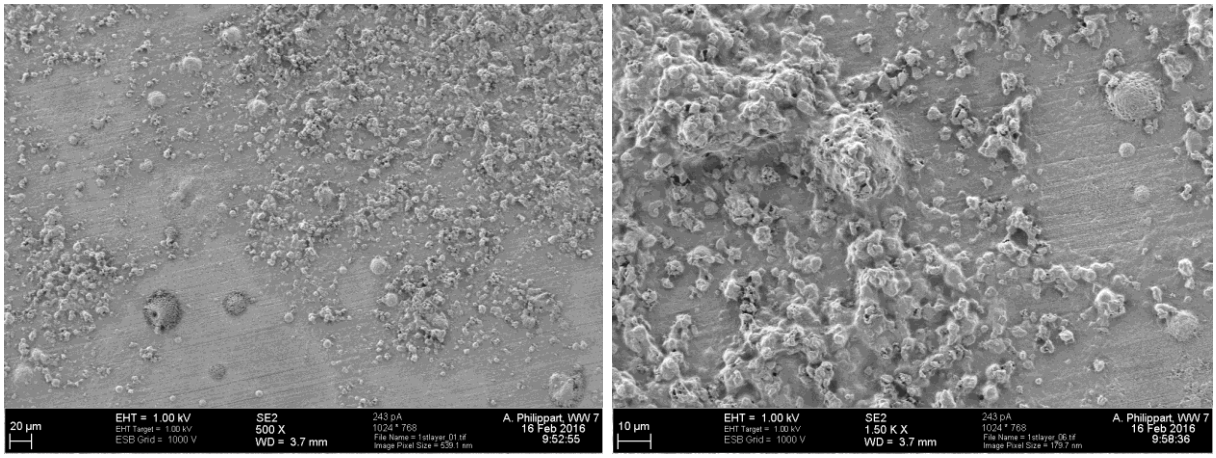

Fig.22 SEM micrograph of the first deposited layer of bioactive glass and chitosan at (left) 500x and (right) 1500x.

Again, the strategy to cover the remaining uncoated areas was to deposit a second layer.

The suspension used for applying a second layer was the CS-Silica suspension. Figure 23 shows the optical microscopic image of the final multi-layer system. A completely covered surface and a small presence of bubbles, is detected. Tearing due to poor adhesion was not macroscopically experienced. SEM images of the coated sample (Figure 24) show the silica particles embedded in the chitosan matrix between larger Bioglass® particles. No significatively large amounts of flaws or cracks were detected.

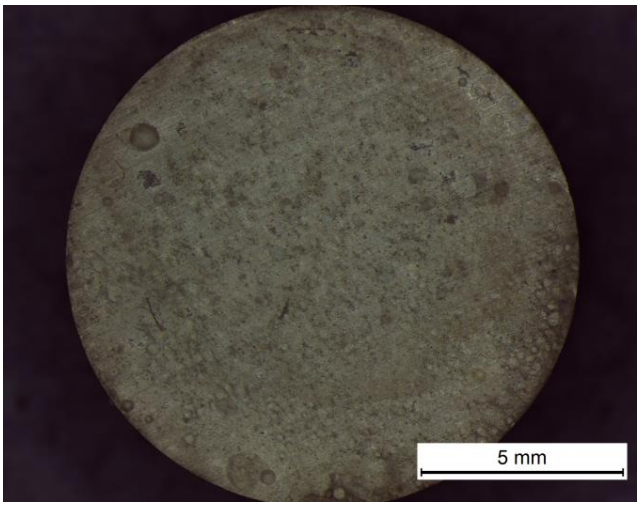

Fig. 23 Optical microscopy of the multi-layer sample, constituted by a first layer of BG-CS and a second layer of CS-Silica.

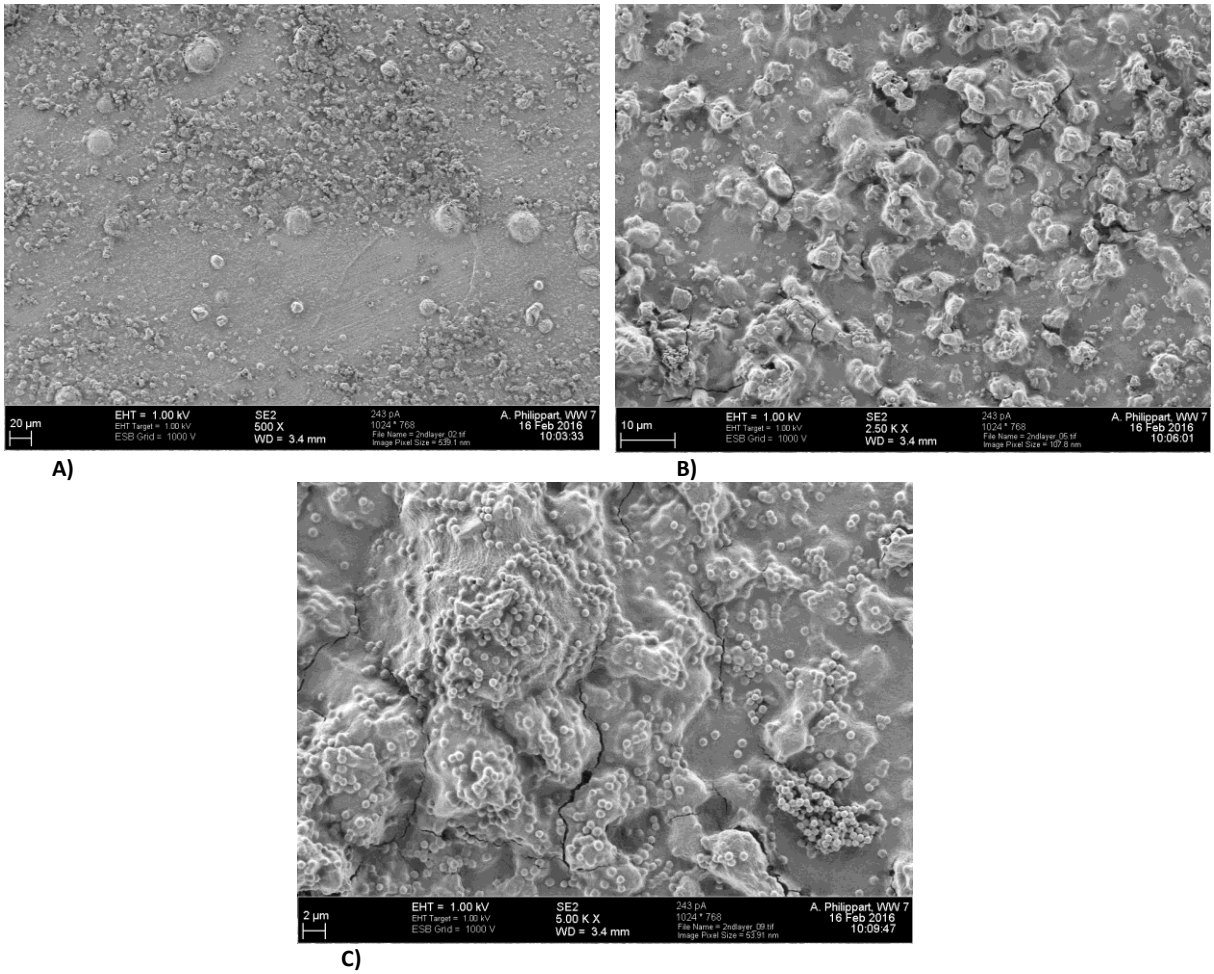

A) **B)**

C)

Fig. 24 SEM image of the multi-layer sample, constituted by a first layer of BG-CS and a second layer of CS-Silica, at (A) 500x, (B)2500x and (C) 5000x.

A layer with the least variety of defects was achieved. Besides, the bioglass particles are of interest in use in biomedical implants because of their osteoconductive and osteoinductive properties, which would result in a rapid bone formation. It has been demonstrated in previous studies that the high density of surface silanol groups (Si-OH) present in amorphous silica induce HCA formation. Besides silica in the silicic acid ($Si(OH)_4$) can chelate aluminum, which its toxicity implicates anemia, impairment of cognitive functions, bone fracture, bone disorder and regenerative bone cells (osteoblast) inactivity [8]. Due to all these reasons, the Bioglass® system was finally selected and was characterized in the following sections to establish and determine its bioactive behavior under conditions similar to that in human body and to study its protective properties.

Table 6 provides a summary of all the systems employed in this project until the final multi-layer system was selected.

Table 6. Summary of the systems employed with the EPD parameters for the first and second deposited layers.

	Silica system		PVA system		Bioglass system
1st layer	CS-Silica		PVA-CS-Silica	Pretreatment* PVA-CS-Silica	CS-BG
EPD parameters	35 V 90 s		40 V 60s	60 V 60s	50 V 60s
2nd layer	CS-Silica	CS	CS	-	CS-Silica
EPD parameters	35 V 90s	30 V 50s	25 V 60s	-	30 V 60s

*CaP pretreatment, explained in detail in Section 4.1.5

Several conclusions can be obtained after analyzing the EPD parameters for the best coatings obtained, presented in Table 6. It is noticeable a decrease or maintenance (in the case of the Silica system) of the EPD parameters for obtaining a suitable second layer. This later can be due to the reduction on the area left to the deposit presence and, consequently, the necessary driving force to generate the coating was decreased. The first layer acts as an insulator, diminishing the driving force for deposition to occur, and is not mistaken to expect an increase on the applied voltage or on the deposition time to generate a second layer. However and due to the obtained results, it may be inferred that the composite layer did not act as a perfect insulator and provided the sufficient driving force to generate a second coating at lower applied voltages.

Regarding the PVA system and comparing the best deposition parameters for the first layer onto the bare sample and onto the pretreated sample, it can be appreciated an increase on the applied voltage for the later one. Then, it can be inferred that the calcium-phosphate layer previously deposited, acted as an effective insulator and made to be necessary to augment the applied voltage to deposit material onto the substrate.

5.3 SURFACE CHARACTERIZATION OF THE SELECTED SYSTEM

The multi-layer system that will be characterized in this section is presented in Table 7.

Table 7. Description of the selected multi-layer coating and the EPD parameters.

Final chosen multi-layer system		
1st layer	Bioactive glass – chitosan	50V 60s
2nd layer	Chitosan – Silica particles	30 V 60s

A technique to evaluate the coatings thickness was not performed in the present project, but, according to previous works developed in the Institute of Biomaterials, it should be in the range of 2µm [7].

Surface characteristics of an implant, such as topography and chemistry, affect the material ability to adsorb water and proteins and consequently to interact with cells and bacteria. The evaluation of wettability is an important factor to take into account, since this property is determinant for the initial protein attachment, relevant for the intended biomedical applications in bone replacement implants. Highly hydrophilic surfaces have shown in previous studies [12] that they are not beneficial for protein adsorption. This phenomenon is explained considering that a highly hydrophilic surface creates hydrogen bonds with the water molecules in the first steps of implant-body fluid interaction. Proteins, in order to be adsorbed onto the surface, must displace water molecules, with certain energy consumption. Beneficial contact angle for bone regeneration applications should be in the range between 35° and 80°[2], while the optimum contact angle to improve blood protein adsorption is considered to be 55°[2]. In Figure 25 can be seen the drops during the contact angle test in the bare alloy (Fig. 25-left) and in the coated substrate (Fig.25-right). Table 8 shows the results obtained for both samples with their corresponding standard deviation.

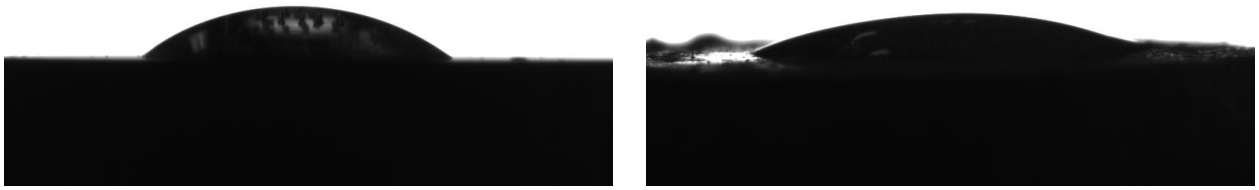

Fig. 25 Deionized water drops during contact angle measurement on the (left) bare alloy and the (right) coated substrate.

Table 8. Contact angle measurements of the bare alloy and the coated substrate.

	Bare alloy	Coated sample
Contact angle/°	57 ± 2	27±2

The contact angle for the bare alloy resulted to be 57° and for the coated substrate was 27°. It is observed a significant decrease in contact angle (i.e.: the hydrophilicity resulted to be augmented). On one side, bioactive glass and the silica particles impart a hydrophilic character to the coating since they have surface-bounded silanol groups (Si-OH). On the other side, chitosan presents a hydrophobic character. The wettability of the coating could be influenced by the contribution of these materials, which possesses different hydrophilic behavior and the greater or

lower affinity with water will depend on their concentration. As the results for the coated substrate showed an increase on hydrophilicity, it can be thought that the concentration of bioactive glass and silica particles was higher than the concentration of chitosan, providing a hydrophilic character. In addition and beyond chemistry of the coating, surface topography and porosity can also influence the wettability behavior [25]. The contact angle for the coated sample resulted to lay out the beneficial contact angle range between 35° and 80°. However, even though the coated surface is not between the beneficial contact angles range for protein adsorption, this does not directly means that the surface will inhibit cell adhesion. The combination of a low hydroxylation degree with low wettability results in low cell adhesion [12].

Besides hydrophilicity, surface roughness is also an essential surface characteristic to promote effective cell adhesion and rapid bone formation to the tissue implant.

The arithmetical average value of the roughness profile (Ra) for the bare sample is presented in Table 9. Since there was no coating deposition on the bare alloy, the Ra value (0.07µm) is directly ascribable to the peaks and valleys left by the grinding process.

Table 9. Arithmetical average value of the roughness profile.

	Bare alloy
Ra average /µm	0.07 ± 0.01

The Ra value for the coated sample presented a high standard deviation so it was not representative. It was presented instead the surface topography in different zones of the substrate (Figure 26 and Figure 27). As observed in both figures, the increment of the surface roughness values compared to that of the bare alloy is approximately one magnitude order. This later could be attributed to the heterogeneous deposition of materials caused by the EPD process, which induced waviness on the surface. Figure 26 shows several peaks and valleys with different high. The abrupt jumps on the peak values are due to Bioglass® and silica particles, with sizes of 2 µm and 0.16 µm respectively, which raise and influence notably the topography. Figure 27 is presented to show the presence of a much higher peak of approximately 15µm, which could be ascribed to particle agglomeration. The presence of agglomerates was previously confirmed through the SEM images.

Rough surfaces involve a larger surface area, allowing a firmer mechanical link to the surrounding tissues and promoting favorable cellular response [13]. The higher roughness observed on the coated samples in comparison with the bare alloy may be beneficial for apatite formation to occur.

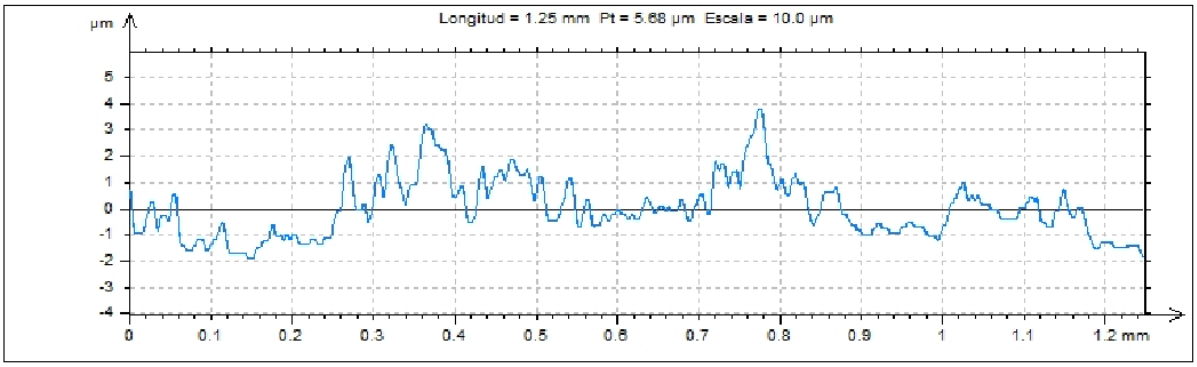

Fig. 26 Surface topography of the coated sample.

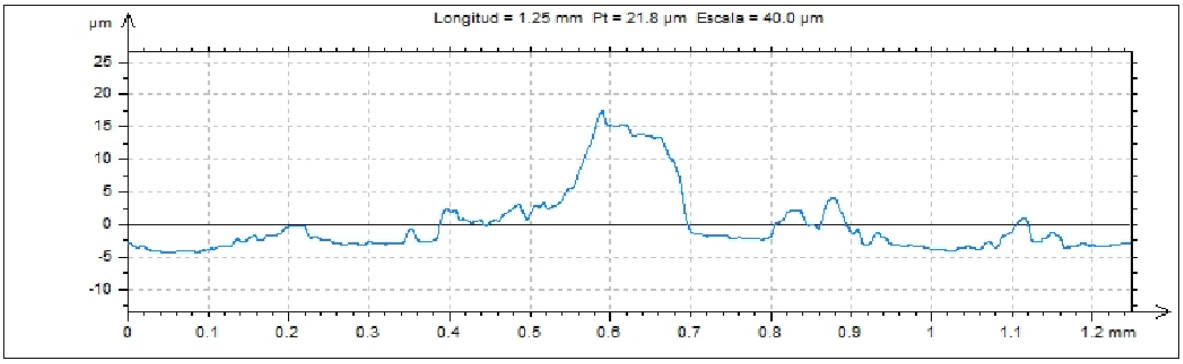

Fig. 27 Surface topography of the coated sample showing particles agglomeration.

A strong adhesion to the metallic surface is of interest as it is important for a safe handling of the product.

Both coatings on the Mg WE43 alloy (with the two layer system) were not peeled off after tape test (Figure 28). The coatings did not show any kind of structural damage or detachment indicating, qualitatively, that the adhesion strength to the substrate is acceptable.

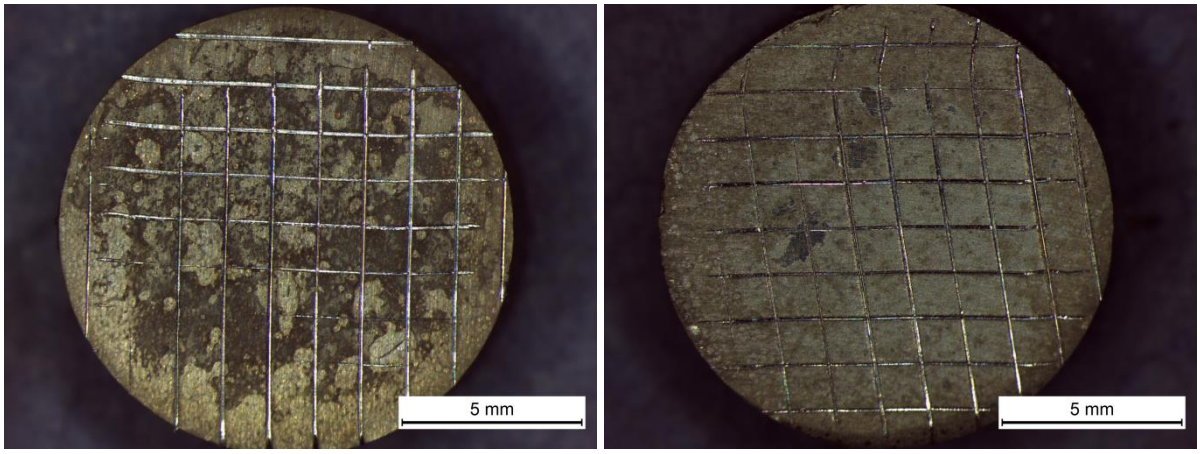

Fig. 28 Surface micrograph after tape test for the (left) first and (right) second layer.

5.4 *IN VITRO* CHARACTERIZATION

For non-coated Mg alloys typically highly non-uniform dissolution takes place over the surface. For coated samples corrosion may start at certain defect present in the coating and therefore also be non-uniform. After corrosion initiation at defects starts, fracture and flaking off of the coating could take place by dissolution propagation.

In organic based coatings there is a risk of corrosion taking place between the coating and substrate, which may lead to detachment of the coating. Even though development of the "perfect" barrier coating for biodegradable Mg alloys may not be required, the coatings should provide sufficient corrosion protection for a given application, and they should lead to a well-defined degradation rate and dissolution behavior.

In an effort to detect which corrosion product was formed on the Mg surface after immersion in 0.1 M NaCl, optical microscopy and Raman spectroscopy were performed. In Figure 29 are presented the optical microscopy images of the bare alloy (Fig.29- left) and the coated sample (Fig. 29- right). As can be observed for the bare alloy, the corrosion product formed on its surface had a uniform and yellow tonality and it appeared distributed all over the surface. The lack of impediments to grow (e.g. the lack of the coating) allowed the products to freely nucleate on the Mg surface and forming a compact layer. The surface of the coated sample after immersion in NaCl during 30 min presented several differences respect to the bare alloy. The formed layer on the surface now appears to be localized in determined areas and the tonality had also changed to a darker color, indicating perhaps that there were more amounts of deposits in these areas.

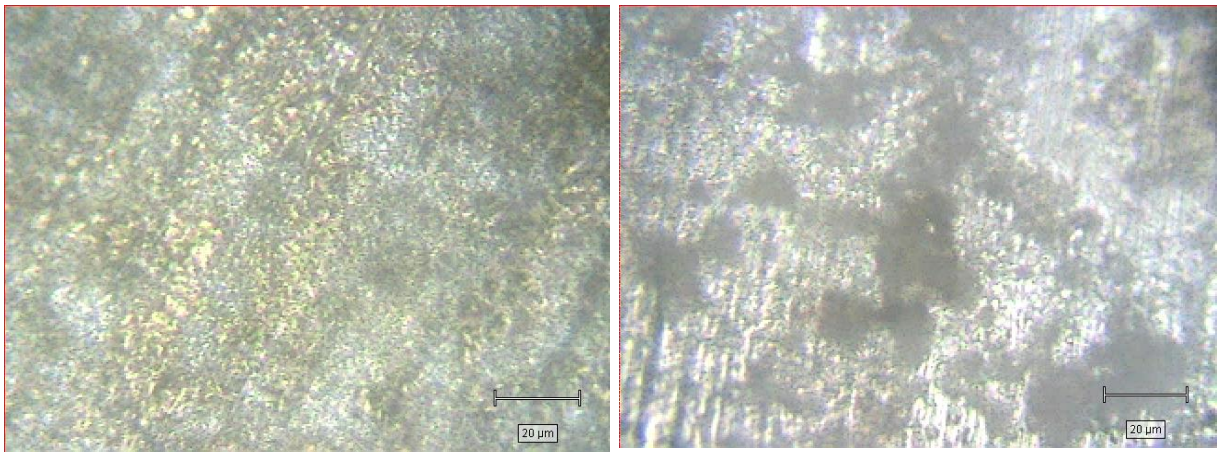

Fig. 29 Surface appearance of the bare alloy (left) and the coated sample (right) after immersion in NaCl during 30 min.

The Raman spectroscopy results are presented in Figure 30. The surfaces of the bare alloy and the coated sample were characterized in the distinct zones. The spectra for the bare alloy presented, both the white and yellow zones observed in the optical microscopy image, the same

spectrum (Fig.30- left). The characteristic peak of $Mg(OH)_2$ is observed at 445 cm^{-1}, confirming that the formed layer was composed of $Mg(OH)_2$ and also that it was present on the entire surface. For the coated sample, instead, the white (i.e. the coating) and the darker areas presented different spectra. The darker zone was ascribed as $Mg(OH)_2$ due to appeareance of the characteristic peak of the hydroxide at 445 cm^{-1}. Besides, this peak is seen with greater intensity than the peak present in case of the bare alloy, inferring that the amount of deposits were greater in the coated sample. The white areas on the multi-layer system presented no peak at lower wavenumbers, confirming that there were no presence of the $Mg(OH)_2$. The broad and high peaks at wavenumbers greater than 1100 cm^{-1} present in the bare alloy are deduced to be ascribed to the MgWE43 substrate, since there is no coating present and the oxides show no adsorption at these wavenumbers.

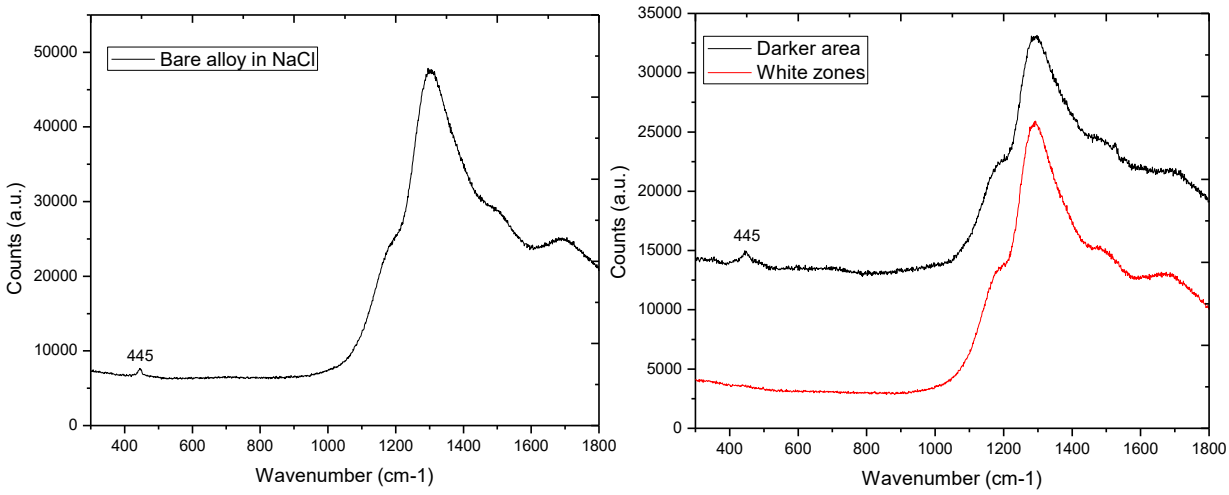

Fig. 30 Raman spectrum of the bare alloy (left) and of the coated sample (right) after immersion in NaCl.

These later results have shown that during immersion in 0.1M NaCl during 30 minutes, a layer of $Mg(OH)_2$ is formed on the surface of the bare alloy. On the other side, $Mg(OH)_2$ was also formed in the surface of the coated sample but in localized areas, forming more dense areas of magnesium hydroxide. At this immersion time, the $Mg(OH)_2$ did not form a continuous layer on the coated sample. A possible explanation could be that the $Mg(OH)_2$in the coated sample nucleated in different localized zones, such as on the metalic substrate, whithin and above the coating, not been able to generate a continuous layer over the surface at this immersion time.

Optical microscopy of the coated sample after 7 days of immersion in SBF is observed in Figure 31. Corrosion of the sample is evidenced by the loss of the original circular shape and consequently, formation of waviness on the border. The surface is characterized by formation of two different distinct zones/deposits: a great amount of a white deposit, which in the later sections will be confirmed to be $Mg(OH)_2$, and a grey or darker area, which will be investigated to determine its bioactive behavior by HA formation.

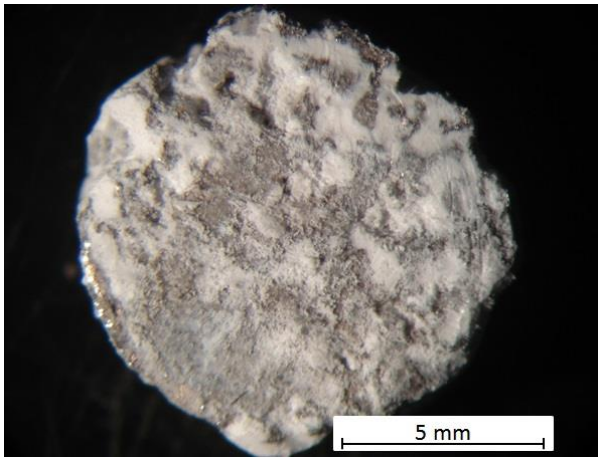

Fig.31 Surface micrograph of the coated sample after immersion in SBF during 7 days.

Figure 32 corresponds to the SEM images of the coated sample after immersion in SBF during 7 days. Figure 32– left, corresponds to the SEM image of the grey area. It is well-known that degradation of materials starts in grain boundaries or in defects because the necessary energy to occur is lower than in bulk. The wide grooves observed in this image correspond to the Mg degradation starting at the grain boundaries. The signs of observing the degrading Mg surface suggest that the coating was dissolved almost completely after immersion in SBF during 7 days. The yellow circles delimitates possible deposits which have a similar morphology to that of typical HA. EDS to determine the composition of such deposits were not carried out in this final project and therefore, is not possible to confirm whether they are HA crystallites or not. Figure 32 –right, presents the SEM image of the white deposit. In this image and in comparison to Figure 32-left, the grain boundaries of the Mg alloy are not detected and instead, it is observed a huge amount of $Mg(OH)_2$ deposit, which covers a great area in an inhomogeneous way.

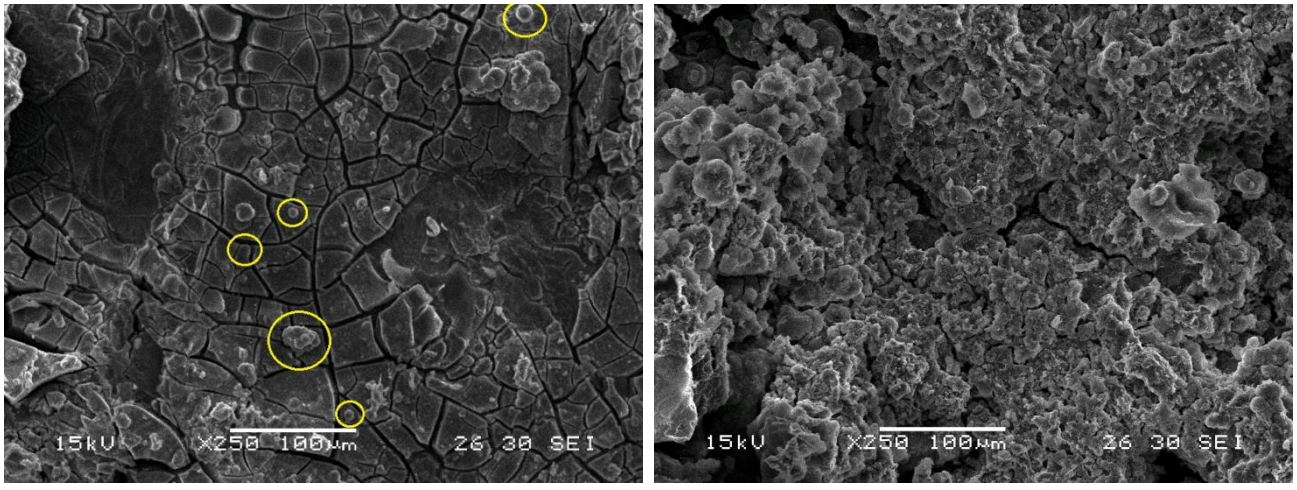

Fig.32 SEM images of the coated sample after immersion in SBF during 7 days at 250x. (Left) Image corresponding to the grey zone in Figure 29. The yellow circles delimitates possible HA crystallites. (Right) $Mg(OH)_2$ white deposits.

During immersion in SBF, the pH value of the solution was registered at different times. Measurement of pH is not an indication of bioactivity behavior but is a way to understand how ion release may be occurring, necessary for the HA formation.

Figure 33 shows the time dependence of the pH when immersed the samples in SBF. There is a rapid increase on the pH value within the first day of immersion and afterwards, pH continues increasing but in a lower rate until it reaches a plateau at approximately 9.7. The rise on the pH value of the surrounding solution can be associated with the degradation of the Mg substrate, by the H_2O reduction and Mg oxidation. Also a controlled release of Ca, P and Na ions from the surface of Bioglass® produced an alkaline pH, which is required for the chemical bonding of hard tissue [42]. In Section 2.3.1.1 was presented the mechanism of HCA formation from bioactive glasses and the first step on Bioglass® dissolution involved a rapid ion exchange of Na^+ and/or Ca^{2+} with H^+ from the SBF solution, which leads to OH^- ions formation. This later could be the reason why there is a rapid alkali increase on pH at short SBF immersion times. The chitosan polymer matrix may delay the Bioglass® dissolution. As stated in the Pourbaix diagram of Mg (not presented in the present work), at pH higher than 8.5, the alkaline medium stimulates the $Mg(OH)_2$ formation. Consequently, pH increase above 8.5 was also attributed to Mg corrosion.

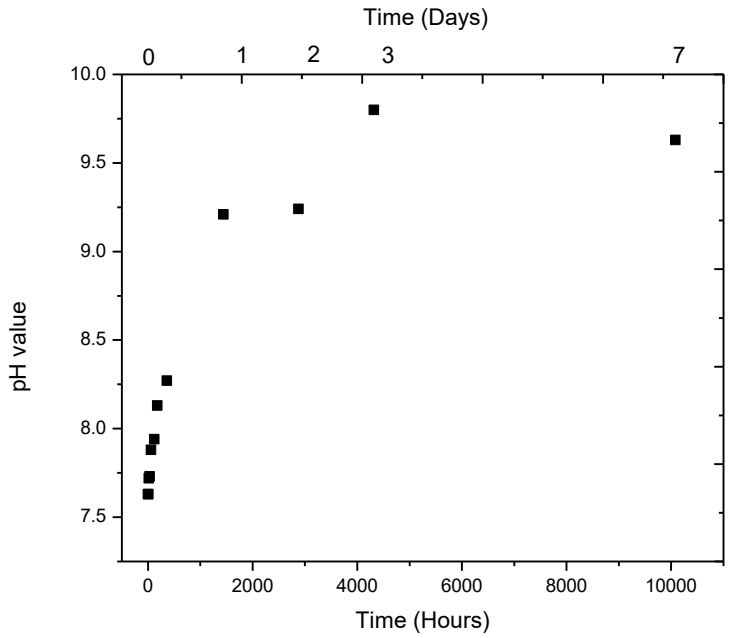

Fig. 33 Time dependence of pH changes associated with the soaking of the material in SBF. Error bars were omitted because they were lower than 5%.

FTIR characterization was performed after 0, 2h, 1, 2, 3 and 7 days of immersion in SBF to investigate it bioactive behavior, which is determined by formation of hydroxyapatite

($Ca_{10}(PO_4)_6(OH)_2$) on the surface of the substrate. The superposition of all the spectra is shown in Figure 34.

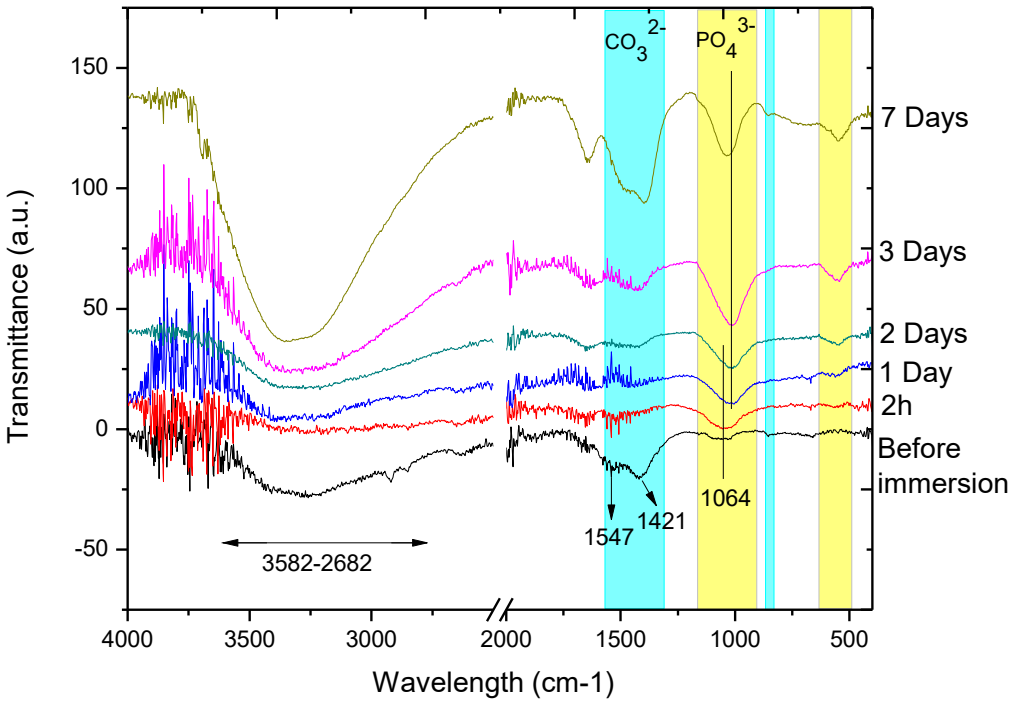

Fig. 34 FTIR spectra of the coated sample before immersion and after 2h, 1, 2, 3 and 7 days of immersion in SBF.

The presence of Bioglass®, chitosan and silica particles was confirmed by the FTIR spectroscopy spectrum of the sample before immersion in SBF, showing the characteristic peaks of chitosan, silica and Bioglass® particles, and revealing the stretching and bending of the bonds present in the molecular structures. Chitosan characteristic peaks were found in:- a broad band between 3582 and 2682 cm^{-1}due to -$NH_2$and O-H stretching; - bending vibrations of the amide II band at1547 cm^{-1} indicating the N-H- vibrations[43]; - stretching of the C-H bond from the -CH_2 and -CH_3groups at 2912 cm^{-1} and 2846 cm^{-1}respectively [26][44]; -bending of the –C-OH bonds at 1421 cm^{-1}; -stretching of the C=O bond at 1064 cm^{-1} and at 857 $cm^{-1}$is present a peak corresponding to stretching of the C-O-C of the saccharide structure [45]. The peak at 1064 cm^{-1} is also referring to the stretching of the Si tetrahedral from bioactive glass and the silica particles [46]. Bending of the O-P-O group in Bioglass® at 590 cm^{-1}[45] is not observed, and could be because is hindered by other functional groups.

The characteristic peaks of HA formation are delimitated by blue and yellow rectangular areas (carbonate and phosphates groups, respectively). For the evaluation of carbonated HA formation, phosphate and carbonates bonds are of interest. Phosphate groups show four modes that are active in the infrared region: -bending vibration of PO_4^{3-} at 560-610cm^{-1} and 430-460cm^{-1}; -asymmetric stretching: a broad band at 1000-1150 $cm^{-1}$and at 960 cm^{-1}. Carbonate bonds from

carbonated HA are sometimes difficult to evaluate for composites materials with polymer matrix such as chitosan as the polymer also has peaks in the same region (C-O high and low energy vibrations between 1410-1470 and 850-890 cm^{-1}, respectively)[22].

If it is paid special attention on the peak around 1000-1150cm^{-1} for the different immersion times in SBF spectrum it can be seen that there is a significantly increase on its intensity and a slight shift to higher wavelength values. This later is due to the dissolving silica, which consequently produces the progressive disappearance of the characteristic peak at 1064cm^{-1} in the spectra, and at the same time due to the increasing formation of the calcium-phosphates, it is formed a characteristic peak at approximately 1030cm^{-1}, assigned to the asymmetric stretching of the PO_4^{3-} group[22]. After 2 days of soaking the sample in SBF, it can be seen the formation of a new peak at 547cm^{-1}, corresponding to the bending vibration of PO_4^{3-} and which continue augmenting its intensity with increasing immersion time. This implies a continuous growing of a phosphate-rich phase. In addition, the spectra of the samples showed an increase in intensity of the carbonate bands at 1421cm^{-1} with time and the emergence of a new peak at 846cm^{-1} after 7 days of soaking. The first carbonate band is characteristic of bending vibration while the second band attributes to a stretching vibration of the C-O liaisons in carbonate groups. The presence of these two carbonate bands and the phosphate bands indicated progressive formation of a carbonate -calcium- phosphate deposit, increasing the deposit amount with immersion time in SBF.

In an effort to confirm the HA formation, Raman spectroscopy, the complementary technique of FTIR, was carried out. Optical microscopy results showed two distinct deposits or zones in the coated sample after immersion in SBF: a white deposit and a grey zone. The Raman spectra of the coated sample before and after 7 days of immersion in SBF, for both the white deposit and the grey zone, are presented for comparison in Figure 35. The 300 – 1800 cm^{-1} spectral range was considered because the main peaks of silicate glasses and HCA fall within this interval [47].A closer overview of Figure 35 is shown in Figure 36 for a better visualization of the characteristic peaks at low wavenumbers. The corresponding assignment to each peak is summarized in Table 10. The spectrum of the unreacted coating shows a peak of low intensity at 933 cm^{-1} corresponding to the P-O symmetric stretching of the O-P-O groups from bioactive glass. The weak intensity of the P-O from Bioglass® may be due to the highly intensive peaks from silica and chitosan, which hinders the phosphate group.

In HCA the position of the P-O stretching peak from the phosphate group appears shifted towards higher wavenumbers and is centered in 960cm^{-1}[48]. In the Raman spectrum of the grey area from the sample after 7 days of immersion in SBF can be observed this shift and the peak is finally centered in 956cm^{-1}. Therefore, can be confirmed the presence of a calcium-phosphate

similar to that of HA. Formation of a new peak at 802cm^{-1} was due to the Si-O-Si stretching from non-dissolved silica or Bioglass® particles. Previously this peak was not observed and may have been because of the intensive peak at 1276cm^{-1}, which may have hindered it.

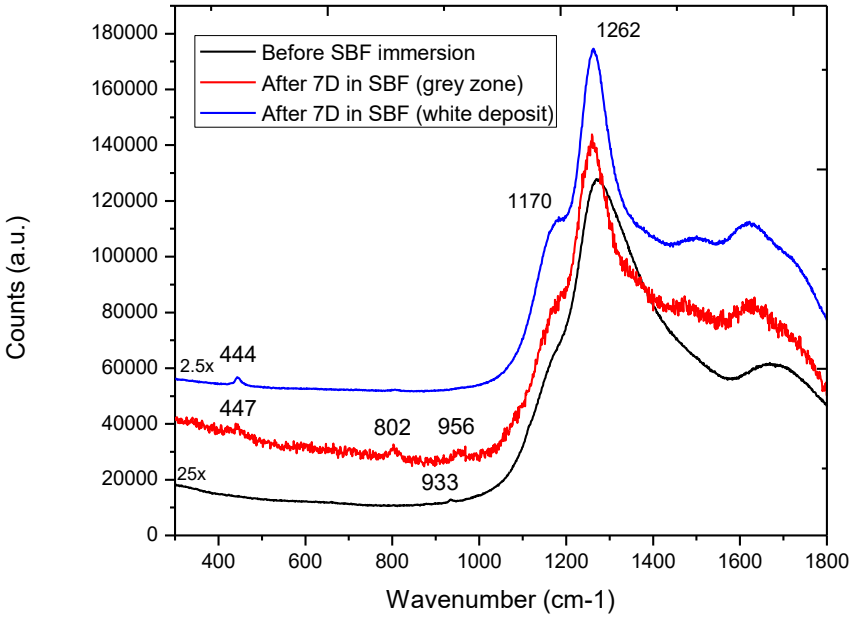

Fig.35 Raman spectra of the samples before immersion in SBF (black line) and after immersion in SBF. The red line corresponds to the spectrum of the grey zone, and the white line white deposit.

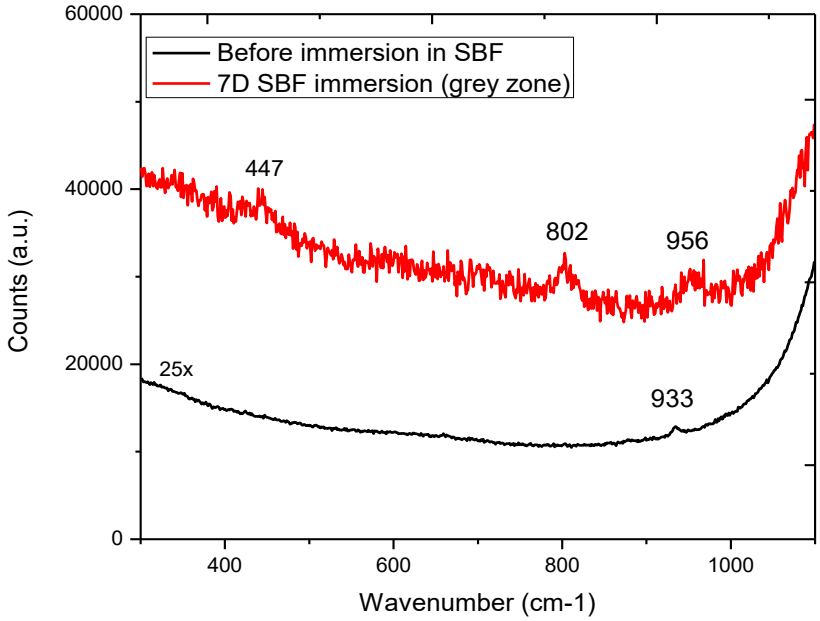

Fig.36 Raman spectrum of the samples before and after immersion in SBF.

Table 10. Assignation to the peaks observed in the Raman spectra.

Peak Wavenumber (cm^{-1})	Assignation	Reference
444-447	$Mg(OH)_2$	[49]
802	Si-O-Si stretching from Silica	[50]
933	P-O symmetric stretching from bioactive glass	[47]
956	P-O symmetric stretching of PO_4^{3-} in HCA	[48]

The Raman spectra of the white deposit from the sample after immersion in SBF presented a peak at 444 cm^{-1}, which is ascribed to $Mg(OH)_2$, the corrosion product from the Mg substrate.

In conclusion, the coated sample after immersion in SBF presented a white deposit consisting on $Mg(OH)_2$ and a grey deposit which is ascribed to a calcium-phosphate similar to HA, non-dissolving silica based particles and $Mg(OH)_2$.

Figure 37 shows the XRD pattern of the coated sample before and after 7 days immersion in SBF. The presence of crystalline hydroxyapatite was confirmed by use of the XRD spectrum of the sample after 7 days of immersion in SBF.

In the spectrum of the coated surface before immersion in SBF can be seen only the characteristic peaks of magnesium (#96-901-3059). The Bioglass® and silica particles possess an amorphous cristalline structure so it is to expect that their spectra not appear in an XRD measurement. Regarding chitosan, due to is polymer nature, could be semicristallyne, but it does not appear in this spectrum. This could be explained because either the chitosan is completely amorphous or the magnesium spectrum hinders the chitosan spectrum. In the spectrum of thesample after 7 days of immersion in SBF (7D-Surface) can be observed new,weakbut broader peaks, identified as $Mg(OH)_2$ (#96-210-1440), the Mg corrosion product. This result is consistent with the obtained Raman measurments. In this spectrum, the intensity of the Mg peaks is much higher than the peaks corresponding to $Mg(OH)_2$, so in order to avoid interference of the Mg phase spectrum, the coating was peeled off with a spatula and it was obtained the resultant XRD measurement (7D-Coating). Now the Mg phase is not seen in the spectrum, the $Mg(OH)_2$ phase is seen with higher intensity and can be appretiated three new peaks corresponding to crystalline apatite (#96-110-0067).

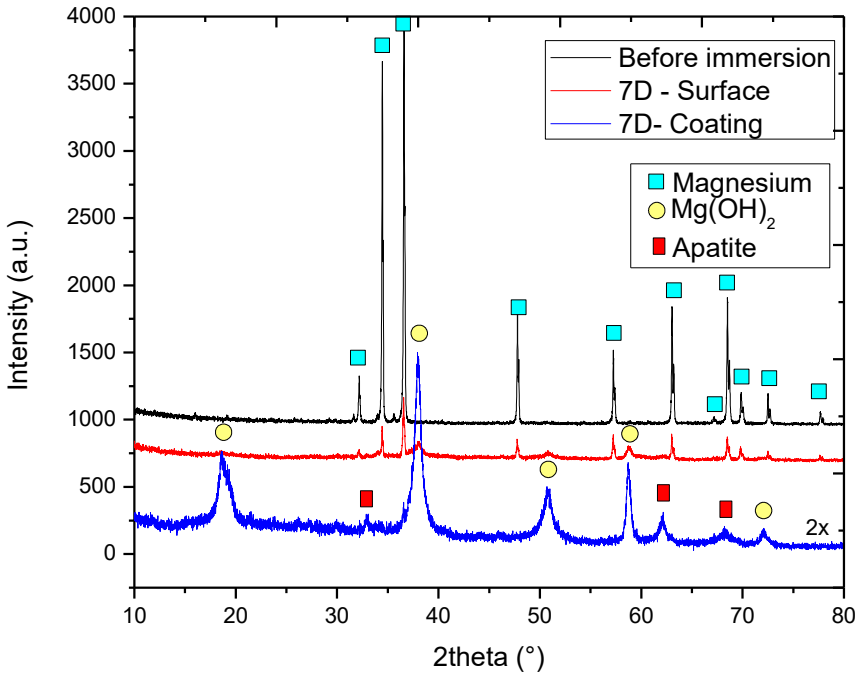

Fig.37 XRD pattern of the coated substrate before and after immersion in SBF during 7 days.

The obtained results from the employeed techniques (SEM, Optical Microscopy, FTIR, Raman and XRD) resulted to be consistent between them, showing the progressively formation of calcium phosphates depositswith immersion time in SBF. Through Raman spectroscopy was confirmed the appeareance of a calcium-phosphate similar to HA due to the characteristic P-O peak from the phosphate group at 956cm^{-1}.The dissappearance of the P-O peak from phosphate group in Bioglass® at 933cm^{-1}indicated that the glass particulares were dissolved and formed the HA. Eventhough SEM images could not assure the presence of HA deposits, XRD ended up to confirm theformation of crystalline HA.

Electrochemical tests were performed in order to evaluate the protective properties of the coating agains corrosion of the substrate. Figure 38 shows the potentiodynamic anodic curve for the bare WE43 alloy and the coated sample after immersion in 0.1M NaCl for 30 minutes. Its worth to notice that the studied Mg alloy and the coated Cs-Silica-BG samples presented a stabilization of the corrosion potential after 30 minutes of immersion in 0.1M NaCl. In the surrounding of the corrosion potential, the polarization curve of the coated sample presented a slight decrease on corrosion potential, oppositely at it would be expected. The later means that the coated surface provides a higher difference potential for corrosion to occur and therefore the driving force is increased. This behaviour could be explained with the inhomogeneities and porous structure of the coating. This coating structure may generate zones with different electrolite concentrations (solution trapt in porous or defects), which ended up generating ocluded cells on the surface of the sample. The presence of this concentration cells formed on the coated sample helps to generate a change in the

surface potencial and hence, the deterioration of the coated samples by enhancing degradation. Also, the possible presence of cracks or pores within the coating, which diminish the area in contact with the electrolyte, may have increased the corrosion rate. The pores or cracks possibly present within the coating may be ascribed to volumetric contraction occuring during the drying process and also because of hydrogen evolution of the metallic surface during corrosion. At greater applied voltagesand until 0 V the two substrates behaved in the same way. In order to appretiate the difference between both curves at low current densities, Figure 38 presents the polarization curves at lower voltages than the maximum reached applied voltage during the potentiodynamic anodic polarization method.

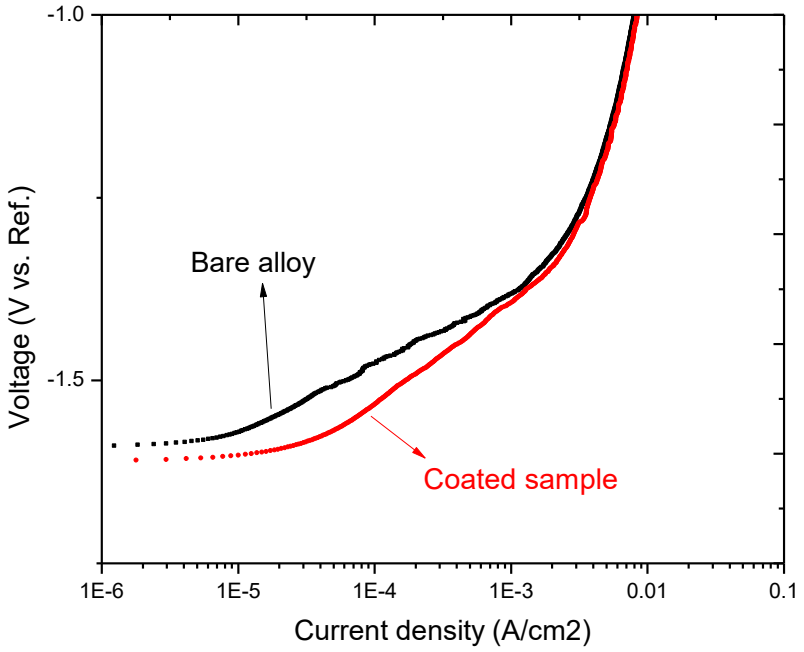

Fig. 38 Polarization curves of the bare alloy and the coated substrate immersed in 0.1M NaCl.

Figure 39 shows Nyquist (left) and Bode (right) plots, as Electrochemical Impedance Spectroscopy (EIS) representation, for the bare alloy and the coated sample after immersion in 0.1 M NaCl for 30 minutes.

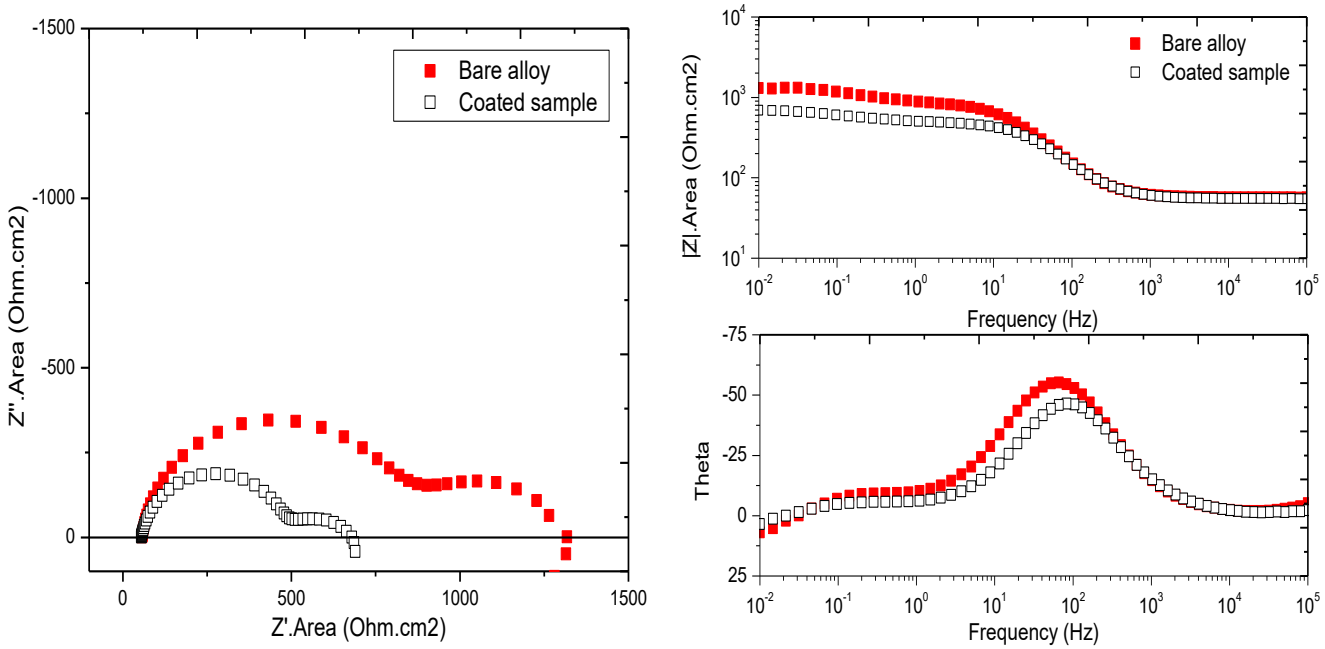

Fig. 39 Nyquist (left) and Bode (right) plots for the bare alloy and the coated substrate.

For the bare WE43 alloy and the coated sample, Nyquist plots consisted in two semi-circles. In the case of the bare alloy, the smaller semi-circle at low frequencies indicates the formation of a porous-oxide layer on the surface, and the bigger semi-circle at high frequencies corresponds to the resistance and capacitance of the electrochemical double-layer. In the case of the coated sample, the smaller semi-circle at low frequencies represents the electrochemical double layer, while the second semicircle indicates the presence of the coating and the corrosion products. Additionally, an inductive loop at low frequencies for both samples can be seen and is ascribed to dissolution of the Mg substrate under the formed layer or to adsorbed ions on the substrate[51].The total resistance for both systems is easily observed at low frequencies in the Bode plot (Figure 39 right)(|Z| vs. frequency) extrapolating to 0 Hz. Noticeable are the rather good results for the bare sample, indicating that maybe there is a formation of a compact layer over the substrate surface, as it was observed in Raman assays, providing better protective properties than the coating in NaCl after 30 min of immersion. In addition, the lack of protective effectiveness of the coating compared to the bare surface could be ascribed to the porosity of the coating that conducts to localized corrosion.

EIS data are generally analyzed in terms of an equivalent circuit model. The equivalent circuit models for both the bare alloy and the coated substrate are presented in Figure 40 left and right, respectively. The elements employed in both circuit models are the same, but the main difference between them is their physical significance. R_{sol} is resistance of the ionic solution, which depends on the ionic concentration, type of ions, temperature, and the geometry of the area in which current is carried. An intact coating can be physically interpreted as an ideal capacitor, but very often

capacitors in EIS do not behave ideally. Instead, they act as constant phase elements (CPE) or leaking capacitors, were the efficiency of the capacitor is not 100%. In the case of the bare alloy, the corrosion products act as a CPE, defined as CPE_{ox} in the equivalent model. For the coated sample, the CPE_c refers to the CPE behavior of the coating itself. R_{po} is the denominated pore resistance, the resistance of ion conducting paths that develop in the coating. These paths can be physical pores filled with the electrolyte and it is assumed that an area of the coating was peeled off and a pocket filled with electrolyte has formed. This electrolyte can be very different than the bulk solution. The interference of this pocket of solution and the bare metal is modeled as a double-layer CPE (CPE_{dc}) in parallel with a kinetically controlled charge-transfer reaction (R_{dc})[52].

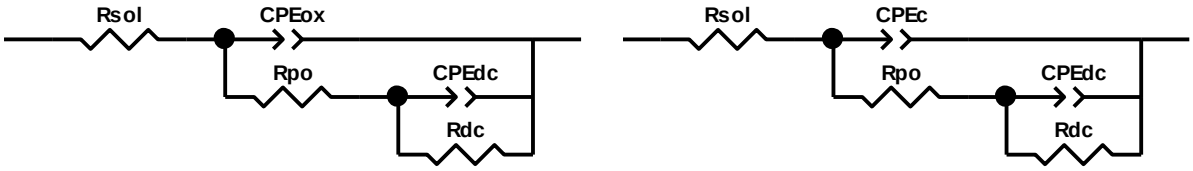

Fig. 40 Equivalent circuit for fitting EIS data of (left) the bare alloy and (right) the coated substrate.

Figure 41 depicts with points the EIS data and with lines the fitting results of the proposed equivalent circuit model. It is possible to observe that the model is well-fitted to the EIS data. The fitting has been done considering an error lower than 10%.

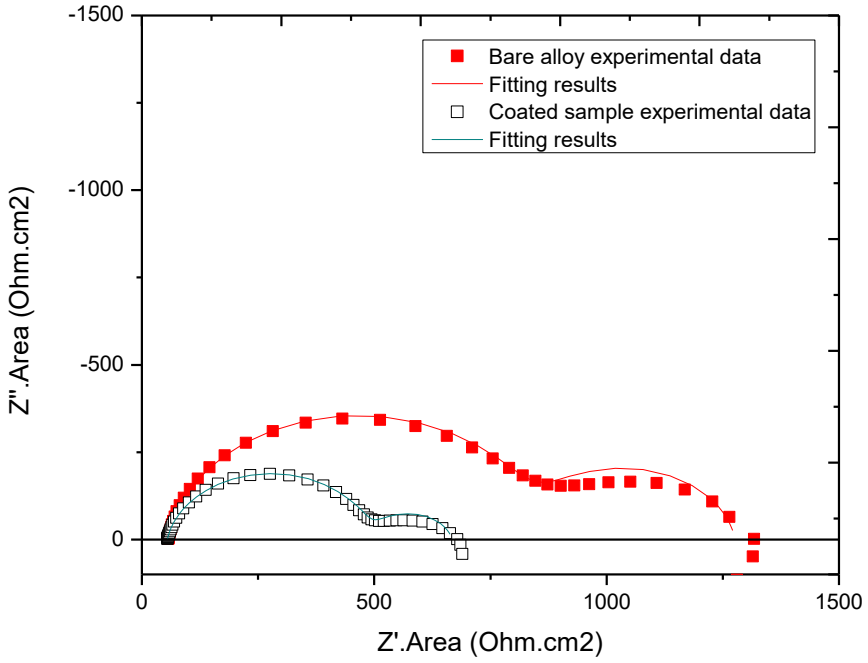

Fig.41 Nyquist plot of the experimental EIS data from bare alloy and the coated sample (points) and the corresponding fitting with the circuit equivalent model (lines).

CPE is described according to the following Equation[53]:

$$CPE = 1/T(j\omega)^{P} \quad \text{(Eq.11)}$$

Where *T* corresponds to the CPE pseudo- capacitance value, ω is the frequency and *P* is related to the system inhomogeneity. A CPE-P value less than 1 indicates the system shows behavior that has been attributed to surface heterogeneity or to continuously distributed time constants for charge transfer reactions, i.e.: the system does not behave as an ideal capacitor [53].

Table 11 presents the values of the elements corresponding to the fitting of the EIS data with the proposed equivalent model.

The effective capacitance associated with the CPE was calculated using Equation 12, which takes into account a parallel array[53].

$$C_{eff} = T^{1/P}(R_{sol}^{-1} + R_{po}^{-1})^{(P-1)/P} \quad \text{(Eq.12)}$$

Where *T* corresponds to the CPE_c-T value and *P* to the CPE_c-P.

Table 11. Values of the physical elements from the equivalent circuits corresponding to the fitting of the EIS data for the bare alloy and the coated sample.

Element	Bare alloy	Coated sample
R_{sol} ($\Omega.cm^2$)	60±4	60±3
CPE_c-T ($\Omega^{-1}.cm^{-2}.s^n$)	$2.1x10^{-5} \pm 2x10^{-6}$	$2.7x10^{-5} \pm 3x10^{-6}$
CPE_c-P	0.917 ± 0.003	0.897±0.005
R_{po} ($\Omega.cm^{-2}$)	1000±200	400±70
C_{eff} (F/cm^{-2})	$1.2x10^{-5} \pm 1x10^{-6}$	$1.3x10^{-5} \pm 1x10^{-6}$
CPE_{dc}-T ($\Omega^{-1}.cm^{-2}.s^n$)	$1.8x10^{-3} \pm 3x10^{-4}$	$5.3x10^{-3} \pm 3x10^{-4}$
CPE_{dc}-P	0.84 ± 0.02	0.807±0.009
R_{dc} ($\Omega.cm^2$)	600±100	163 ±5

The polarization resistance (R_p) was calculated for the bare alloy and for the coated sample by use of Equation 13.

$$R_p = R_{po} + R_{dc} \quad \text{(Eq.13)}$$

Table 12. Polarization resistance values for the bare alloy and the coated sample.

	Bare alloy	Coated sample
Rp ($\Omega.cm^2$)	1600±300	563±75

From the calculated values of the polarization resistance values can be noticed that the bare alloy presents a higher R_p, indicating a greater current flow restriction through the formed layer than through the coating itself. The C_{eff} calculated values were similar for both the bare alloy and the coating sample. Therefore, the corrosion products layer demonstrated to achieve better protective corrosion properties than the multi-layer coating.

The effective capacitance is possible to relate it to the film thickness *d* according to [53]:

$$Ceff = \frac{\varepsilon.\varepsilon 0.A}{d} \quad \text{(Eq.14)}$$

Where ε is the dielectric constant, ε0=8.8542x10^{-12}F/m is the permittivity of vacuum and *A* is the exposed area.

The thickness of the coating was not calculated by Equation 14 due to the lack of a specific value for the dielectric constant and because of an undetermined area of exposed metal due to porosity and inhomogeneities of the coating. Considering ε=10 [54] for the bare alloy and the C_{eff} previously calculated, the thickness of the film formed on the bare alloy in 0.1M NaCl after 30 min was 73nm. This result reveals the existence of a very thin (in the nano metric scale) $Mg(OH)_2$ layer at this immersion time. The presence of the magnesium hydroxide as a corrosion product in 0.1M NaCl in the bare alloy and the coated sample was confirmed by Raman spectroscopy at the beginning of this section.

Therefore, can be assured that the coating, initialy, does not provides better protective properties to corrosion, possibly because of ocluded cells formation and/or cracks and pores, which localize corrosion, incrementing in this way the degradation process in comparison to the bare alloy. This statement can only be assured for 30 minutes of immersion in 0.1M NaCl.

6 CONCLUSIONS

As a general conclusion for the present final project it is possible to affirm that research and investigation has been done with the purpose of trying to tackle several drawbacks of the Mg WE43 alloy, which nowadays make it impossible to use in the biomedical field. The diverse characterization methods and techniques employed allowed the understanding of their operation and use, and allowed to extract the relevant information that was used to obtain conclusions and formulate new hypothesis.

As particular conclusions can be highlighted:

- Silica particles were successfully synthetized. By controlling the amount of reactants in the solutions from the sol-gel method, it could be synthetized monodispersed and spherical silica particles with the desired size.
- The chitosan/silica/bioactive glass composite coatings were deposited on the Mg WE43 alloy through Electrophoretic Deposition. Variation of the involved deposition parameters between ranges of 15-85V and 20-90s allowed analyzing and selecting, through optical microscopy and SEM, the best multi-layer coating.
- Analysis of a variety of characterization tests allowed the identification of hydroxycarbonate apatite formation after 7 days of immersion of the coated sample in Simulated Body Fluid at 37°C, indicating its bioactive behavior.
- The electrochemical tests made possible to determine that the coating did not provide improvements on protection against corrosion at least until 30 minutes of immersion in 0.1M NaCl at ambient temperature.

7 FUTURE WORK

The proposed further research on the present project is:

- Employment of AC – EPD (Alternating Current - Electrophoretic Deposition) to deposit material instead of DC-EPD, to tackle the mayor drawback of EPD method: water hydrolysis. Alternating current involves the movement of electric charges that periodically reverse direction. AC conditions generates that potentials that drive the electrochemical reactions also drive the current that flows through the double layer capacitance formed at the electrode-electrolyte interface. Hence, when frequency of the applied field is sufficiently high, almost all current flows through the double layer capacitance and the decomposition of water becomes too low for gas bubbles to form [55]. AC- EPD involves a greater number of parameters than in DC, such as frequency, voltage peak-to-peak, deposition time and the shape of the waveform. It is therefore proposed a Taguchi design of Experiment to avoid the time-consuming, costly and inefficient work methodology of the trial- and –error method of DC-EPD.

- Determination of the thickness of the final coating by use of FIB-SEM.

- Evaluation of electrochemical tests at longer immersion times and in different electrolytes (i.e. SBF, DMEM, Hank) to determine if the multi-layer coated sample could develop sometime better protective properties than the bare alloy. If the $Mg(OH)_2$layer still provides better protective properties than the coating itself, it is proposed to corrode intentionally the surface of the Mg alloy before deposition of the coating.

- Development of a single-layer coating with the same objectives of the present project in order to reduce processing time and costs.

- Evaluation of the mechanical integrity loss of the substrate with immersion time.

- Further *in vitro* tests to evaluate cytotoxicity and cellular adhesion.

- Tests on *in vivo* conditions.

8 REFERENCES

[1] T. Rzychoń and A. Kiełbus, "Microstructure of WE43 casting magnesium alloy," *J. Achiev. Mater. Manuf. Eng.*, vol. 21, no. 1, pp. 31–34, 2007.

[2] I. Corni, N. Neumann, S. Novak, K. König, P. Veronesi, Q. Chen, M. P. Ryan, and A. R. Boccaccini, "Electrophoretic deposition of PEEK-nano alumina composite coatings on stainless steel," *Surf. Coatings Technol.*, vol. 203, no. 10–11, pp. 1349–1359, 2009.

[3] K. Grandfield and I. Zhitomirsky, "Electrophoretic deposition of composite hydroxyapatite-silica-chitosan coatings," *Mater. Charact.*, vol. 59, no. 1, pp. 61–67, 2008.

[4] H. Hornberger, S. Virtanen, and A. R. Boccaccini, "Biomedical coatings on magnesium alloys - A review," *Acta Biomater.*, vol. 8, no. 7, pp. 2442–2455, 2012.

[5] B. Neirinck, O. Van Der Biest, and J. Vleugels, "A current opinion on electrophoretic deposition in pulsed and alternating fields," *J. Phys. Chem. B*, vol. 117, no. 6, pp. 1516–1526, 2013.

[6] Q. Chen, L. Cordero-Arias, J. A. Roether, S. Cabanas-Polo, S. Virtanen, and A. R. Boccaccini, "Alginate/Bioglass?? composite coatings on stainless steel deposited by direct current and alternating current electrophoretic deposition," *Surf. Coatings Technol.*, vol. 233, pp. 49–56, 2013.

[7] F. Pishbin, A. Simchi, M. P. Ryan, and A. R. Boccaccini, "Electrophoretic deposition of chitosan/45S5 Bioglass composite coatings for orthopaedic applications," *Surf. Coatings Technol.*, vol. 205, no. 23–24, pp. 5260–5268, 2011.

[8] L. Borum and O. C. Wilson, "Surface modification of hydroxyapatite. Part II. Silica," *Biomaterials*, vol. 24, no. 21, pp. 3681–3688, 2003.

[9] S. Bhat and A. Kumar, "Biomaterials and bioengineering tomorrow ' s healthcare," *Landes Biosci.*, vol. 3, no. September, pp. 1–12, 2013.

[10] P. Tengvall and I. Lundström, "Physico-chemical considerations of titanium as a biomaterial," *Clin. Mater.*, vol. 9, no. 2, pp. 115–134, 1992.

[11] K. Anusavice, "Dental Ceramics," *Phillips' Sci. Dent. Mater.*, pp. 655–720, 2003.

[12] S. Spriano, V. Sarath Chandra, A. Cochis, F. Uberti, L. Rimondini, E. Bertone, A. Vitale, C. Scolaro, M. Ferrari, F. Cirisano, G. Gautier di Confiengo, and S. Ferraris, "How do wettability, zeta potential and hydroxylation degree affect the biological response of biomaterials?," *Mater. Sci. Eng. C*, 2016.

[13] F. Javed, H. B. Ahmed, R. Crespi, and G. E. Romanos, "Role of primary stability for successful osseointegration of dental implants: Factors of influence and evaluation.," *Interv. Med. Appl. Sci.*, vol. 5, no. 4, pp. 162–167, 2013.

[14] S. Shadanbaz and G. J. Dias, “Acta Biomaterialia Calcium phosphate coatings on magnesium alloys for biomedical applications : A review,” *Acta Biomater.*, vol. 8, no. 1, pp. 20–30, 2012.

[15] M. P. Staiger, A. M. Pietak, J. Huadmai, and G. Dias, “Magnesium and its alloys as orthopedic biomaterials: A review,” *Biomaterials*, vol. 27, no. 9, pp. 1728–1734, 2006.

[16] S. Agarwal, J. Curtin, B. Duffy, and S. Jaiswal, “Biodegradable magnesium alloys for orthopaedic applications: A review on corrosion, biocompatibility and surface modifications,” *Mater. Sci. Eng. C*, vol. 68, pp. 948–963, 2016.

[17] S. Heise, S. Virtanen, and A. R. Boccaccini, “Review Article Tackling Mg alloy corrosion by natural polymer coatings — A review,” pp. 1–14, 2016.

[18] L. Jiang, F. Xu, Z. Xu, Y. Chen, X. Zhou, G. Wei, and H. Ge, “Biodegradation of AZ31 and WE43 magnesium alloys in simulated body fluid,” *Int. J. Electrochem. Sci.*, vol. 10, no. 12, pp. 10422–10432, 2015.

[19] D. A. Jones, *Principles and Prevention of corrosion*. New York: Macmillan Publishing Company, 1992.

[20] I. Zhitomirsky, “Electrophoretic deposition of organic – inorganic nanocomposites,” no. October, pp. 8186–8195, 2006.

[21] A. Boccaccini, J. Roether, and B. Thomas, “The Electrophoretic Deposition of Inorganic Nanoscaled Materials-A Review,” *J. Ceram. Soc. Japan*, vol. 14, no. 1, pp. 1–14, 2006.

[22] I. Notingher, J. R. Jones, S. Verrier, I. Bisson, P. Embanga, P. Edwards, J. M. Polak, and L. L. Hench, “Application of FTIR and Raman spectroscopy to characterisation of bioactive materials and living cells,” *Spectrosc. Int. J.*, vol. 17, no. 2–3, pp. 275–288, 2003.

[23] L. L. Hench, “The story of Bioglass,” *J. Mater. Sci. Mater. Med.*, vol. 17, no. 11, pp. 967–978, 2006.

[24] J. R. Jones, “Acta Biomaterialia Review of bioactive glass : From Hench to hybrids,” *Acta Biomater.*, vol. 9, no. 1, pp. 4457–4486, 2013.

[25] Q. Chen, S. Cabanas-Polo, O. M. Goudouri, and A. R. Boccaccini, “Electrophoretic co-deposition of polyvinyl alcohol (PVA) reinforced alginate-Bioglass?? composite coating on stainless steel: Mechanical properties and in-vitro bioactivity assessment,” *Mater. Sci. Eng. C*, vol. 40, pp. 55–64, 2014.

[26] M. Mehdipour and A. Afshar, “A study of the electrophoretic deposition of bioactive glass-chitosan composite coating,” *Ceram. Int.*, vol. 38, no. 1, pp. 471–476, 2012.

[27] T. Wilson, *EFFECTS OF SILICA BASED BIOMATERIALS by*. 2011.

[28] K. S. Rao, K. El-Hami, T. Kodaki, K. Matsushige, and K. Makino, “A novel method for synthesis of silica nanoparticles,” *J. Colloid Interface Sci.*, vol. 289, no. 1, pp. 125–131, 2005.

[29] S. Wang, X. Wang, F. G. Draenert, O. Albert, H. C. Schröder, V. Mailänder, G. Mitov, and W. E. G. Müller, “Bioactive and biodegradable silica biomaterial for bone regeneration,” *Bone*, vol. 67, pp. 292–304, 2014.

[30] W. Li, Y. Ding, R. Rai, J. A. Roether, D. W. Schubert, and A. R. Boccaccini, “Preparation and characterization of PHBV microsphere/45S5 bioactive glass composite scaffolds with vancomycin releasing function,” *Mater. Sci. Eng. C*, vol. 41, pp. 320–328, 2014.

[31] J. Mota, N. Yu, S. G. Caridade, G. M. Luz, M. E. Gomes, R. L. Reis, J. A. Jansen, X. Frank Walboomers, and J. F. Mano, “Chitosan/bioactive glass nanoparticle composite membranes for periodontal regeneration,” *Acta Biomater.*, vol. 8, no. 11, pp. 4173–4180, 2012.

[32] M. Kumar, “A review of chitin and chitosan applications,” *React. Funct. Polym.*, vol. 46, no. 1, pp. 1–27, 2000.

[33] “Thermo Phisics Scientific.” [Online]. Available: https://www.thermofisher.com/ar/es/home/industrial/spectroscopy-elemental-isotope-analysis/spectroscopy-elemental-isotope-analysis-learning-center/molecular-spectroscopy-information/ftir-information/ftir-basics.html.

[34] G. S. Bumbrah and R. M. Sharma, “Raman spectroscopy ??? Basic principle, instrumentation and selected applications for the characterization of drugs of abuse,” *Egypt. J. Forensic Sci.*, vol. 6, no. 3, pp. 209–215, 2016.

[35] J. Przondziono, W. Walke, E. Hadasik, and J. Szala, “Corrosion Resistance Tests of Magnesium Alloy We43 After Extrusion,” vol. 52, no. 2, pp. 243–246, 2013.

[36] J. H. Zhang, P. Zhan, Z. L. Wang, W. Y. Zhang, and N. B. Ming, “Preparation of monodisperse silica particles with controllable size and shape,” *J. Mater. Res.*, vol. 18, no. 3, pp. 649–653, 2003.

[37] S. Heise and V. Wagener, “Developing surface pre-treatments for electrophoretic deposition of biofunctional chitosan-bioactive glass coatings on a WE43 magnesium alloy,” *Appl. Surf. Sci.*, 2017.

[38] T. Kokubo and H. Takadama, “How useful is SBF in predicting in vivo bone bioactivity?,” *Biomaterials*, vol. 27, no. 15, pp. 2907–2915, 2006.

[39] L. Besra and M. Liu, “A review on fundamentals and applications of electrophoretic deposition (EPD),” *Prog. Mater. Sci.*, vol. 52, no. 1, pp. 1–61, 2007.

[40] U. K. Parida, “Synthesis and Characterization of Chitosan-Polyvinyl Alcohol Blended with Cloisite 30B for Controlled Release of the Anticancer Drug Curcumin,” *J. Biomater. Nanobiotechnol.*, vol. 2, no. 4, pp. 414–425, 2011.

[41] N. Iqbal, R. Nazir, A. Asif, A. A. Chaudhry, M. Akram, Y. F. Goh, A. Akram, R. Amin, S. H. Park,

and R. Hussain, “Electrophoretic deposition of PVA coated hydroxyapatite on 316L stainless steel,” *Curr. Appl. Phys.*, vol. 12, no. 3, pp. 755–759, 2012.

[42] L. L. Hench and H. a Paschall, “Direct chemical bond of bioactive glass-ceramic materials to bone and muscle.,” *J. Biomed. Mater. Res.*, vol. 7, no. 3, pp. 25–42, 1973.

[43] S.-M. Lai, A. J.-M. Yang, W.-C. Chen, and J.-F. Hsiao, “The Properties and Preparation of Chitosan/Silica Hybrids Using Sol-Gel Process,” *Polym. Plast. Technol. Eng.*, vol. 45, no. January, pp. 997–1003, 2006.

[44] S. A. Samad, S. Md Masum, and M. Moniruzzaman, “Preparation and Characterization of Chitosan from Shrimp shell waste,” *Int. J. Sci. Eng. Res.*, vol. 6, no. 5, 2015.

[45] X. Bui, H. Oudadesse, Y. Le Gal, A. Mostafa, G. Cathelineau, U. M. R. Cnrs, U. De Rennes, and G. Leclerc, “Microspheres of Chitosan-Bioactive Glass for Application in Orthopedic Surgery . In vitro experiment.”

[46] M. S. Sadjadi, F. Najafizadeh, S. G. Fateami, M. K. Mobarakeh, R. M. Afshar, B. S. Faculty, I. Azad, and O. Surgery, “The effect of Silica coating on bioactivity and biodegradability of Hydroxyapatite synthesized in collagen matrix,” *Int. J. Bio-Inorganic Hybrid Nanomater.*, vol. 5, no. 1, pp. 19–26, 2016.

[47] D. Bellucci, G. Bolelli, V. Cannillo, A. Cattini, and A. Sola, “In situ Raman spectroscopy investigation of bioactive glass reactivity: Simulated body fluid solution vs TRIS-buffered solution,” *Mater. Charact.*, vol. 62, no. 10, pp. 1021–1028, 2011.

[48] L. L. Hench, N. Roki, and M. B. Fenn, “Bioactive glasses: Importance of structure and properties in bone regeneration.,” *J. Mol. Struct. - Elsevier*, vol. 1074, pp. 24–30, 2014.

[49] E. . de Oliveira and Y. Hase, “Infrared study and isotopic effect of magnesium hydroxide.,” *Elsevier*, pp. 53–56, 2001.

[50] A. Bertoluzza, C. Fagnano, M. Antonietta Morelli, V. Gottardi, and M. Guglielmi, “Raman and infrared spectra on silica gel evolving toward glass,” *J. Non. Cryst. Solids*, vol. 48, no. 1, pp. 117–128, 1982.

[51] V. Wagener and S. Virtanen, “Protective layer formation on magnesium in cell culture medium,” *Mater. Sci. Eng. C*, vol. 63, pp. 341–351, 2016.

[52] “Basics of Electrochemical Impedance Spectroscopy.” [Online]. Available: https://www.gamry.com/application-notes/EIS/basics-of-electrochemical-impedance-spectroscopy/.

[53] B. Hirschorn, M. E. Orazem, B. Tribollet, V. Vivier, I. Frateur, and M. Musiani, “Determination of effective capacitance and film thickness from constant-phase-element parameters.,” *Electrochim. Acta - Elsevier*, pp. 6218–6227, 2010.

[54] H. Duan, C. Yan, and F. Wang, “Effect of electrolyte additives on performance of plasma electrolytic oxidation films formed on magnesium alloy AZ91D,” *Electrochim. Acta*, vol. 52, no. 11, pp. 3785–3793, 2007.

[55] A. Chávez-Valdez and A. R. Boccaccini, “Innovations in electrophoretic deposition: Alternating current and pulsed direct current methods,” *Electrochim. Acta*, vol. 65, pp. 70–89, 2012.


UNIVERSIDAD NACIONAL
DE MAR DEL PLATA


FACULTAD DE INGENIERIA


FAU
FRIEDRICH-ALEXANDER
UNIVERSITÄT
ERLANGEN-NÜRNBERG
TECHNISCHE FAKULTÄT